# Estimation of spatial distribution of coastal ocean primary production in Hiroshima Bay, Japan, with a geostationary ocean color satellite

Asaoka, Satoshi
Nakada, Satoshi
Umehara, Akira
Ishizaka, Joji
Nishijima, Wataru

(Citation)
Estuarine, Coastal and Shelf Science,244:106897

(Issue Date)
2020-10-05

(Resource Type)
journal article

(Version)
Accepted Manuscript

# Estimation of spatial distribution of coastal ocean primary production in Hiroshima Bay, Japan, with a geostationary ocean color satellite

Satoshi ASAOKA[a]*, Satoshi NAKADA[b], Akira UMEHARA[c],

Joji ISHIZAKA[d], Wataru NISHIJIMA[c]

a Research Center for Inland Seas, Kobe University

5-1-1 Fukaeminami, Higashinada, Kobe, 658-0022 JAPAN

b Center for Regional Environmental Research, National Institute for Environmental Studies

16-2 Onogawa, Tsukuba, 305-8601 JAPAN

c Environmental Research and Management Center, Hiroshima University

1-5-3, Kagamiyama, Higashihiroshima, Hiroshima, 739-8513 JAPAN

d Institute for Space-Earth Environmental Research, Nagoya University

Furo, Chikusa, Nagoya, 464-8601 JAPAN

*Corresponding author:

Tel & Fax: +81-78-431-6357, E-mail: s-asaoka@maritime.kobe-u.ac.jp

Address: Research Center for Inland Seas, Kobe University, 5-1-1 Fukaeminami, Higashinada, Kobe, 658-0022 JAPAN

**Abstract**

Ocean primary production measured by conventional methods using carbon isotope are mostly calculated from point sampling, which is not appropriate for estimating the temporal and spatial variations involved in marine ecosystems. Ocean color remote sensing can estimate spatial variation of ocean primary production at the global scale. However, the spatial resolution of the ocean color remote sensing is not adequate for estimating coastal ocean primary production. This study sought to establish a novel methodology for estimating coastal ocean primary production in Hiroshima Bay, Japan using high-resolution ocean color data (~500 m) and higher temporal resolution (hourly during the day) obtained by a geostationary ocean color satellite, GOCI-COMS. Estimated values of primary production derived from the ocean color satellite based on the Kameda & Ishizaka model did not correlate with observed primary production. We estimated primary production in Hiroshima Bay with a modified Kameda & Ishizaka model. The coefficient of determination between observed and estimated primary production by the ocean color satellite was 0.750. The slope of the linear regression was 1.00, and root mean square error was 165 mg-C $m^2$ $d^{-1}$. Our proposed method was thus sufficient for discussions of the changes in spatial distribution of primary production in Hiroshima Bay. Finally, spatial distribution of primary production in Hiroshima Bay was

estimated using our proposed method. In January, the primary production of the Hiroshima Bay ranged <50-1000 mg-C $m^{-2}$ $d^{-1}$, and increased to 1000-1600< mg-C $m^{-2}$ $d^{-1}$ during seasonal blooms in spring and autumn. The primary production was relatively high at the innermost and western parts of the bay which affected by terrigeneous loads compared to other parts of the bay. In July 2016, highest primary production was observed at the innermost of the bay, ranging from 1200–1600< mg-C $m^{-2}$ $d^{-1}$. The high primary production was considered to be due to the supply of nutrients from terrigeneous load. Hence, our proposed method based on the high-resolution (approx. 500 m) ocean-color product has been enabled us to estimate primary production in coastal seas including complicated topographic areas such as enclosed seas or channels of less than 1 km wide.

**Key Words**

Carbon fixation, Coastal sea, Chlorophyll, Food chain, GOCI/COMS, Remote sensing

## Highlights

- Coastal primary production was estimated using a geostationary ocean color satellite.
- GOCI-COMS was used to estimate primary production in Hiroshima Bay, Japan.
- The root mean square error of estimated primary production was 165 mg-C $m^2$ $d^{-1}$.
- The proposed algorithm is adequate for the monitoring of coastal primary production.

## 1. Introduction

Primary production (PP) is the synthesis of organic matter from inorganic substances such as carbon dioxide through photosynthesis or chemosynthesis. In aquatic ecosystems, algae are mainly responsible for PP, and thus support the base of the food chain. Therefore, PP is what is called the starting point of the material cycle in ecosystems. Approximately 45 gigatons of organic carbon is formed by marine phytoplankton each year, 16 gigatons of which are exported to the ocean interior (Falkowski et al., 1998). Therefore, PP by marine phytoplankton plays an important role in the global carbon cycle (Bauer et al., 2013; Siegel et al., 2016). PP is also important in the field of marine ecosystems. The biological productivity of lower trophic levels supports the production of higher trophic levels in food webs. Estimation of PP is therefore an essential step for understanding upper trophic level yields (Friedland et al., 2012). Hence, it is very important to quantify PP to understand the global carbon cycle and marine ecosystems in coastal seas, in addition to open oceans.

PP has conventionally been measured by the $^{14}C$ method, $^{13}C$ method, and oxygen light and dark bottle method (Steeman Nielsen, 1952; Hama et al., 1983; Gaarder and Gran, 1927). The $^{14}C$ and $^{13}C$ methods measure uptake rate of $^{13}C$ or $^{14}C$ labeled bicarbonate by photosynthesis of phytoplankton (Steeman Nielsen, 1952). The $^{14}C$ method is sensitive

because it measures $^{14}C$ labeled bicarbonate, which is phytoplankton uptake by photosynthesis, with a scintillation counter. Therefore, the $^{14}C$ method has been widely used to determine PP in, for example, arctic plankton PP (Engel et al., 2013), deep PP (Lyngsgaard et al., 2014) and Antarctic spring bloom PP (Johanna et al., 2015). However, it is difficult to apply the $^{14}C$ method in places such as Japan, where use of radioactive isotopes in the field is strictly controlled.

To measure PP in these areas, the $^{13}C$ method is usually applied. The $^{13}C$ method measures the isotopic balance of $^{13}C$ and $^{12}C$ before and after incubation, and estimates $^{13}C$ uptake by phytoplankton (Hama et al., 1983). The $^{13}C$ method takes a 4-h incubation to enrich $^{13}C$ into phytoplankton, because it is less sensitive than the $^{14}C$ method. In addition, an isotope ratio mass spectrometer is needed to determine the isotope ratio of $^{12}C$ and $^{13}C$. The $^{13}C$ method has also been widely used (Kluijver et al., 2013; Shiozaki et al., 2013; Tsuchiya et al., 2013).

In the light and dark bottle method, PP is estimated from the difference of dissolved oxygen concentration in light and dark bottles after incubation (Gaarder and Gran, 1927). However, this method has low sensitivity. In addition, these methods all involve time-consuming incubation to measure PP in the ocean or laboratory. For those reason, most PP is calculated from spot sampling, which is not appropriate for estimating temporal and

127 spatial variations of ocean PP involved in marine ecosystems. In order to estimate
128 temporal and spatial variations, ocean color remote sensing has been proposed (Feldman
129 et al., 1989; Platt and Sathyendranath, 1988; Saino, 1993; Behrenfeld et al., 2006). Ocean
130 color remote sensing enables estimations of temporal and spatial variation in ocean PP on
131 a global scale. However, these studies have been chiefly based on coastal zone color
132 scanner (CZCS) data, in which accuracy of phytoplankton pigment (chlorophyll-a; Chl a)
133 is not sufficient and also data amount is not enough for estimating coastal ocean PP (1-20
134 km; Feldman et al., 1989). Presently, the Sea-viewing Wide Field-of-view Sensor
135 (SeaWiFS) and MODIS were used to estimate oceanic PP, and improved accuracy of Chl
136 a concentration and time resolution of estimating oceanic PP (Bosc et al., 2004; Arrigo
137 and Dijken, 2011). Although, these ocean color remote sensing enabled us to estimate
138 spatial variations of ocean PP on a global scale, spatial resolution was not enough to
139 estimate coastal ocean primary production. The high resolution, less than 1 km mesh was
140 required for estimating coastal ocean PP because coastal ocean includes topographically
141 complicated area such as enclosed seas or channels.

142 To provide a novel methodology for estimation of coastal ocean PP to overcome defects
143 in conventional method, we use a high-resolution ocean color data (~500 m) with
144 modifications which obtained by an ocean color satellite, GOCI-COMS. The Korean

145 geostationary satellite Communication, Ocean and Meteorological Satellite (COMS)
146 equipped with a geostationary ocean color sensor, the Geostationary Ocean Color Imager
147 (GOCI), was launched in June 2010. The GOCI is the world's first geostationary ocean
148 color sensor that can measure radiance from the ocean surface in the visible and near-
149 infrared bands for application to ocean remote sensing (Ryu et al., 2012; Choi et al., 2012).
150 Observations from the GOCI-COMS enabled us to access high-resolution (~500 m) ocean
151 color data, as well as higher temporal resolution (hourly during the day). These
152 specifications are advantageous for estimating the temporal and spatial distribution of
153 coastal ocean production compared to other sensors. The goals of this study were: (1) to
154 establish a novel methodology for estimating coastal ocean PP from high-resolution ocean
155 color data obtained by GOCI-COMS; and (2) to discuss the accuracy of our proposed
156 method by comparison with field observation data; and ultimately (3) to reveal spatial
157 distribution coastal ocean PP in Hiroshima Bay, Japan, using our proposed method.
158
159 **2. Experimental**
160 **2.1 Study area of field observation**
161 We measured the seasonal net PP (four times per year) at 7 sampling stations in
162 Hiroshima Bay, Seto Inland Sea, Japan, between November 2014 and August 2015 (**Fig.**

163 **1**) in order to compare PP obtained by field observations with estimated values from the
164 ocean color satellite (OCS).

165 Hiroshima Bay is a semi-enclosed bay located in the middle west part of the Seto Inland
166 Sea, and measures about 30 km from east to west and 50 km north to south for a total area
167 of 1043 $km^2$, with an average depth of 26 m. Hiroshima Bay is significantly affected by
168 intensive oyster culture (annual production approximately 19,000 tons as meat weight)
169 and terrigeneous loads from the Ohta River (catchment area: 1710 $km^2$). The yearly
170 averaged discharge of the Ohta River is approximately 78.81 $m^{-3}$ $s^{-1}$ (Japan River
171 Association). The terrigenous loads from the Ohta River form halocline in the northern
172 part of the bay every summer. Ohta River input accounts for 90% of total freshwater input
173 to the northern area of Hiroshima Bay. Entrained seawater from the southern area by the
174 estuary circulation is 7-14 times larger than riverine fresh water input in the northern area
175 of the bay (Yamamoto et al., 2000). Anthropogenic activities such as industrialization and
176 urbanization have resulted in frequent summertime red tide since 1970s (Yanagi, 2008).
177 In recent years, red tide occurrence in the bay decreased to only one or two times a year
178 due to intensive reduction of nutrients load. However, the bottom sediments in the
179 northern part of the bay are affected by high organic flux (Asaoka et al., 2018).

180

## 2.2 Sampling procedures of field observation

Training and research vessels, Hikari (National Institute of Technology, Hiroshima College) was used for the observations. Vertical profiles of temperature, salinity, fluorescence and photon flux density were measured using a multi electrode (AAQ176, JFE Advantec, Kobe, Japan).

To measure chlorophyll *a* (Chl a) and PP, 4 L of seawater was collected at depths of 100%, 50%, and 10% surface irradiance with a Van Dorn water sampler. The collected water samples were kept in cool and dark conditions, and transferred to a laboratory.

## 2.3 Sample treatment and analysis

To determine the Chl a concentration in the laboratory, 300 ml of seawater was filtered through glass-fiber filters (GF/F, Whatman, Maidstone, UK), and filter residues were extracted with 10 mL of 90% acetone under dark conditions at -20 °C for 16–24 hours. The extracts were sonicated for 20 min, and Chl *a* concentrations were determined fluorometrically (10-AU-5, Turner Designs, Sunnyvale, CA, USA), according to the Welschmeyer method (Welschmeyer, 1994).

To measure PP, seawater samples were filtered through a 220-µm mesh screen to remove large zooplankton, and then transferred into 500-mL polycarbonate bottles, which

199 regulated light intensity (50% and 10%) using cheesecloth. After the addition of
200 $NaH^{13}CO_3$ (Cambridge Isotope Laboratories, Inc.), bottles were immediately incubated
201 in a water bath at in situ temperature with light intensity of ca. 200 μmol-photons $m^{-2}$ $sec^{-1}$
202 using fluorescent lamps for 4 h. After incubation, the samples were filtered through
203 precombusted (450 ºC, 4 h) GF/F filters, treated with 1 mol $L^{-1}$ HCl for removal of
204 inorganic carbon, and stored at -20 °C until isotope analysis. Particulate organic carbon
205 (POC) and atom% of $^{13}C$ of the residuals on the dried filters (60 °C, 48 h) were analyzed
206 by elemental analyzer-isotope ratio mass spectrometer (FlashA EA1112-DELTA V
207 Advantage, Thermo Fisher Scientific, MA, USA). The photosynthetic rate was calculated
208 according to Hama et al., (1983).
209
210 **2.4 Estimation of primary production from field observation**
211 Primary production was estimated by following Umehara et al., 2018. Chl a specific
212 productivity was estimated as
213
214 $$PB = PR / CHL \quad \cdot \cdot \cdot (1)$$
215
216 where *PB*, *PR* and *CHL* are Chl a specific productivity (mgC $mgChl.a^{-1}$ $h^{-1}$),
217 photosynthetic rate (mgC $m^{-3}$ $h^{-1}$), and Chl a concentration (mgChl.a $m^{-3}$), respectively.

PP in the euphotic zone (surface to depth of 1% surface irradiance) of the each station were obtained using the following equations:

$$PP_{STN} = 12 \times \int (PB_Z \times CHL_Z) dz \cdot \cdot \cdot (2)$$

$$PB_Z = a \times \left(\frac{I_Z}{I_0}\right) \times 100 \cdot \cdot \cdot (3)$$

where $PP_{STN}$, $PB_Z$ and $CHLz$ are PP in the euphotic zone at each station (mgC $m^{-2}$ $d^{-1}$), Chl *a* specific productivity at a depth of Z m (mgC mgChl.$a^{-1}$ $h^{-1}$) and Chl a concentration (mgChl.*a* $m^{-3}$) at a depth of Z, respectively. In equation (3), a is a regression coefficient between relative irradiance (%) and Chl a specific productivity in the bay at each seasonal investigation. $I_z$ and $I_0$ indicate photon flux density (μmol-photons $m^{-2}$ $sec^{-1}$) at depth Z, and at the surface, respectively.

**2.5 Estimation of primary production from the ocean color satellite**

GOCI-COMS obtains eight hourly images during the day, and covers approximately 2,500 × 2,500 $km^2$ around the Japanese Islands and Korean Peninsula, centered at 36°N and 130°E with a spatial resolution of ca. 500 m and a very high signal-to-noise ratio (>1000) (Amin et al., 2013). GOCI has six visible bands, centered at 412, 443, 490, 555, 660, and 680 nm, and two near-infrared bands, centered at 745 nm and 865 nm. Level-1

products eight hourly images (9:00AM to 4:00PM) were downloaded from the website of the Korea Ocean Satellite Center (KOSC, http://kosc.kiost.ac/eng/p20/kosc_p21.html). Well-calibrated Level-2 products can be derived from Level-1 data converted with the GOCI Data Processing System (GDPS) developed by the Korea Institute of Ocean Science and Technology (Ryu et al., 2012). Products at 412, 443 and 572 nm were extracted in the study area from 34.40° to 33.90°N and 132.1° to 132.6° E. The acquisition period for GOCI products was from January 2015 to December 2017.

We used the vertically generalized production model (VGPM) established by Behrenfeld and Falkowski (1997) to estimate depth-integrated PP (*IPP*: mg C $m^{-2}$ $d^{-1}$). In the VGPM, *IPP* was calculated as follows:

$$IPP = 0.66125 \; P_{opt}^{B} \; \frac{E_0}{E_0 + 4.1} \; Z_{eu} \; Chl_{opt} \; D_{irr} \quad \cdot \cdot \cdot (4)$$

$$E_{\%}(z) \cong 1 = \exp\{2.3(\kappa sat)z\} \quad \cdot \cdot \cdot (5)$$

$$P_{opt}^{B} = \frac{0.071T - 3.2 \times 10^{-3}T^2 + 3.0 \times 10^{-5}T^3}{Chl_{total}}$$

$$+(1.0 + 0.17T - 2.5 \times 10^{-3}T^2 - 8.0 \times 10^{-5}T^3) \cdot \cdot \cdot (6)$$

where $E_0$ is daily photosynthetically active radiation (PAR) above the sea surface (E $m^{-2}$ $d^{-1}$) obtained by MODIS/AQUA, $Z_{eu}$ (m) is euphotic depth, defined as physical depth at 1% of $E_0$ (m) calculated by equation (5), and *ksat* is the extinction coefficient derived from Level-2 products with GDPS ($m^{-1}$). Photoperiod ($D_{irr}$) is set at 12 h, corresponding to estimation of PP used in field observations (Umehara et al., 2018). Chl a concentration at the sea surface (SSC) is used as daily mean $Chl_{opt}$ (mg $m^{-3}$), which was calculated from hourly Chl *a* concentration obtained by GOCI. The optimal assimilation efficiency of the productivity ($P^B_{opt}$ : mg $m^{-3}$) was defined as equation (6) established by Kameda and Ishizaka (2005), where $Chl_{total}$ (mg $m^{-3}$) is Chl *a* concentration obtained from Level-2 products, Chl*a*. Daily surface temperature (SST) was obtained by MODIS/AQUA.

Chromophoric dissolved organic matter (CDOM: $m^{-1}$) was obtained by Level-2 products from GDPS (Nakada et al., 2018).

*CDOM* (λ=400 nm) was calculated using the remote sensing reflectance ratio of bands 1 ($R_{rs}$ 412 nm) to 4 ($R_{rs}$ 555 nm) with equation (7).

$$CDOM(400)=0.2355R^{-1.3423}\ m^{-1} \quad \cdots (7)$$

where $R=R_{rs}(412)/R_{rs}(555)$

The observed chlorophyll-specific photosynthetic rate as a function of PAR ($P_{obs}$) was

calculated from following equation (8).

$$P_{obs}=0.0109I+0.388 \quad \cdots \quad (8)$$

where $P_{obs}$ is the observed chlorophyll-specific photosynthetic rate (μgC μgChl$a^{-1}$ $h^{-1}$), and $I$ is PAR (μE $m^{-2}$ $s^{-1}$).

## 3. Results and discussion

### 3.1 Accuracy of primary production estimated from the ocean color satellite

PP in Hiroshima Bay estimated from the ocean color satellite (OCS), based on Kameda & Ishizaka (2005) shown in equations (4) – (6), did not correlate with observed PP (coefficient of determination; $r^2$=0.109) indicating that the chlorophyll-specific photosynthetic rate proposed by Kameda & Ishizaka (2005) in equation 6 was not appropriate in Hiroshima Bay. In response to this result, we used an observed chlorophyll-specific photosynthetic rate to estimate PP using the OCS in equation (8), because the Seto Inland Sea is enclosed and affected by significant terrigenous nutrients load, resulting in a chlorophyll-specific photosynthetic rate that is different from the open ocean.

The observed chlorophyll-specific photosynthetic rate used in equation (8) was observed from Hiroshima Bay in autumn when nutrients were not a limiting factor in PP

because the concentration of DIN and DIP in the bay ranged from 3.1-25.3 and 0.4-1.5 μmol $L^{-1}$, respectively. Therefore, in autumn, the chlorophyll-specific photosynthetic rate is controlled by PAR rather than by nutrients. The slope in equation (8) was almost the same as in winter (0.0104) when nutrients were not a limiting factor in PP either.

The water temperature ranged from 20.5 to 21.5 ºC in autumn, and from 9.6 to 11.9 ºC in winter. Because the slope of the chlorophyll-specific photosynthetic rate was almost the same despite the water temperature in Hiroshima Bay, we did not take water temperature into account when calculating the chlorophyll-specific photosynthetic rate used in our proposed model (equation (8)).

When the observed chlorophyll-specific photosynthetic rate calculated by equation 8 was used to estimate PP obtained by equation 4, the coefficient of determination between observed and estimated PP by the OCS improved to $r^2$=0.750 (**Fig. 2**). However, the slope of the linear regression was 0.713, indicating that the PP estimated by OCS was approximately a 28.7% overestimation compared to observed PP.

Other parameters for PP estimation in equation (4) were euphotic depth ($Z_{eu}$), chlorophyll concentration ($Chl_{opt}$), $E_0/(E_0+4.1)$ and photoperiod ($D_{irr}$). Because photoperiod corresponded to the estimation of PP in field observations, we did not take photoperiod into account. Therefore, we compared other parameters from satellite-

310 derived euphotic depth ($Z_{eu}$), chlorophyll concentration ($Chl_{opt}$) , $E_0/(E_0+4.1)$, and
311 observations of in situ. The relationship between the observed euphotic depth and the
312 satellite-derived euphotic depth calculated by equation 5 is shown in **Fig. 3**. The euphotic
313 depth value derived from OCS at Sts. 3 and 4, which are shallow areas (water depth 11~15
314 m) in winter, was estimated to be 27~29 m, high compared to observed water depth. This
315 overestimation might be due to high transparency, which causes underestimation of the
316 extinction coefficient by OCS resulting in the overestimation of euphotic depth. When
317 the euphotic depth derived from OCS at these two stations in winter was excluded from
318 the analysis, the slope of the linear regression was 0.971 ($r^2$=0.658; **Fig. 3**). The accuracy
319 and precision of estimated euphotic depth from the OCS was evaluated by root mean
320 square error (RMSE) (Sasaki et al., 2008). The RMSE and bias of the estimated euphotic
321 depth was 3.2 and -0.19, respectively. Therefore, the euphotic depth derived from OCS
322 was in good agreement with observed euphotic depth.

323 Chlorophyll a concentration ($Chl_{opt}$) is also significant factor in estimating PP. The
324 relationship between observed $Chl_{opt}$ and $Chl_{opt}$ derived from the OCS in Hiroshima Bay
325 is shown in **Fig. 4**. Although a linear relationship was observed between observed Chl a
326 (average concentration of 0-5 m depth) and OCS-derived Chl a ($r^2$=0.835), the slope of
327 the linear regression was 3.46. Therefore, the value derived from the OCS underestimated

328 chlorophyll a concentration (by approximately 1/3) compared to the observed value. The
329 error here was might be attributed to atmospheric correction (Gordon, 1997; Cota et al,
330 2003; Hayashi et al., 2015).

331 When the corrected chlorophyll *a* concentration (3.46 times OCS-derived Chl *a*) was
332 used to estimate PP calculated by equation 4, the slope of the linear regression was 0.206.
333 The PP estimated by OCS was approximately 79% overestimation compared to observed
334 PP.

335 The satellite-derived PAR used in this study ranged from 26.1–54.9 E $m^{-2}$ $d^{-1}$,
336 corresponding to 0.86–0.93 in $E_0/(E_0+4.1)$. Therefore, $E_0/(E_0+4.1)$ was not a significant
337 parameter for estimating PP in equation 4.

338 Hence, the overestimation of PP by the OCS could not be explained by the errors
339 attributed to euphotic depth ($Z_{eu}$), Chlorophyll a concentration ($Chl_{opt}$), or $E_0/(E_0+4.1)$.
340 Therefore, the coefficient (0.66125) in equation (4) was tuned to 0.1362 to be consistent
341 with observed PP. The coefficient used in Kameda & Ishizaka (2005), which was
342 optimized to estimate PP in the open ocean, might not be appropriate for coastal and
343 enclosed waters like Hiroshima Bay. Finally, we estimated PP based on equation (9)
344 modified the equation (4).

345

346 $$IPP = 0.1362P_{obs} \quad \frac{E_0}{E_0 + 4.1} \quad Z_{eu} \;\; Chl_{cor} \quad D_{irr} \quad \cdot\cdot\cdot (9)$$

347

348 $Chl_{cor}$ is used as 3.46 times (in the case of Hiroshima Bay) daily mean Chl a concentration
349 calculated from hourly Chl a concentration obtained by GOCI.

350 Relationship between observed and corrected PP in Hiroshima Bay estimated from the
351 OCS was shown in **Fig. 5**. The coefficient of determination between observed and
352 corrected PP estimated by the OCS was $r^2$=0.750. The slope of the linear regression was
353 1.00. The RMSE, normalized RMSE (%), and bias were 165 mg-C $m^{-2}$ $d^{-1}$, 31.2%, and
354 10.8, respectively. The RMSE of PP was less than the standard deviation (SD: 250) and
355 relative standard deviations (RSD 57%) of observed PP at all stations, indicating that the
356 error of estimated PP by the OCS was smaller than the temporal and spatial distribution
357 of PP in Hiroshima Bay. Therefore, our proposed method is sufficiently accurate for
358 discussions of changes in temporal and spatial distribution of PP in Hiroshima Bay.

359 PP obtained by our proposed model was compared to the previous VGPM developed
360 by Behrenfeld & Falkowski, 1997 and Kameda & Ishizaka, 2005. The RMSE, bias, slope
361 and the coefficient of determination between observed and PP estimated by this study
362 were improved compared to the previous VGPM (**Table 1**). Our proposed model was
363 modified both the chlorophyll a concentration and the chlorophyll-specific photosynthetic

364 rate ($P^B_{opt}$). As mentioned above, the chlorophyll a concentration was corrected to 3.46
365 times GOCI-derived chlorophyll a concentration to compensate for the error of
366 atmospheric correction. The chlorophyll-specific photosynthetic rate in the VGPM
367 proposed by Behrenfeld and Falkowski (1997) was defined as a function of SST. However,
368 the observed chlorophyll-specific photosynthetic rate in Hiroshima Bay was almost the
369 same despite the water temperature. In the case of modified VGPM developed by Kameda
370 and Ishizaka 2005, the chlorophyll-specific photosynthetic rate was a function of SST and
371 chlorophyll concentration at the sea surface considering the phytoplankton community;
372 one was small-sized phytoplankton with high $P^B_{opt}$ and the other was large-sized
373 phytoplankton. The observed phytoplankton community in Hiroshima Bay was mainly
374 composed of *Skeletonema costatum* and *Chaetoceros spp*. which accounted for 47-98%
375 of the total cells (16-23,740 cells $mL^{-1}$) in November, February and August except at Sts.
376 6 and 7 in August. In contrast, 35-87% of phytoplankton was composed of *Leptocylindrus*
377 *danicus* and *Cerataulina sp.* in May (Umehara et al., 2018). Because the dominant species
378 of phytoplankton were only a few diatom species in Hiroshima Bay affected by
379 terrigeneous load, we did not take phytoplankton community into account when
380 calculating the chlorophyll-specific photosynthetic rate. Therefore, the chlorophyll-
381 specific photosynthetic rate calculated by the previous VGPM developed by Behrenfeld

382 & Falkowski, 1997 and Kameda & Ishizaka, 2005 was not appropriate for estimating the
383 chlorophyll-specific photosynthetic rate in Hiroshima Bay. Therefore, we modified the
384 chlorophyll a concentration and the chlorophyll-specific photosynthetic rate to calculate
385 PP. Ultimately, the coefficient (0.66125) in equation (4) was also adjusted to 0.1362 to be
386 consistent with observed PP.
387 We also succeeded in estimating PP at St. 5 which was narrow area (1-3 km)
388 surrounded by islands (**Fig. 1**). The error between observed and estimated PP was 1.3-
389 23%. The high-resolution (~500 m) ocean color data obtained by the GOCI-COMS was
390 advantageous for estimating the spatial distribution of PP.
391
392 **3.2 Monthly variations of primary production in Seto Inland Sea estimated from the**
393 **OCS**
394 We estimated PP in Hiroshima Bay, Japan using a modified Kameda & Ishizaka model
395 proposed in this study.
396
397 **3.2.1 Primary production in 2015 (Fig. 6)**
398 In January, PP at the innermost and western parts of the Hiroshima Bay ranged < 50-
399 400mg-C $m^{-2}$ $d^{-1}$. The PP at the center and southern parts of the bay was 500-1000mg-C

400 $m^{-2}$ $d^{-1}$. This is because, Chl a concentration at the center and southern parts of the bay
401 was 4-8 μg $L^{-1}$, which was higher than that of other areas (0.2-3 μg $L^{-1}$; **Fig. S1**). The SST
402 at the center and southern parts of the bay was also higher than that of other areas (**Fig.**
403 **S2**). Hence, it is considered that the PP at the center and southern parts of the bay was
404 enhanced by the high SST.
405 In February, PP was almost uniformly distributed around the bay, ranging from 300–
406 500 mg-C $m^{-2}$ $d^{-1}$. In March, both PP and CDOM increased to 700–1300 mg-C $m^{-2}$ $d^{-1}$
407 and was 0.12–0.24 $m^{-1}$ at the innermost and western parts of the bay (**Fig. S3**). Because
408 CDOM showed significant negative correlations among observed sea surface salinity
409 (SSS), CDOM is considered one of the powerful indicators of riverine plumes (Nakada
410 et al., 2018). Hence, the innermost and western parts of the bay were substantially affected
411 by terrigeneous load from the Ohta, Oze and Nishiki rivers compared to other areas. At
412 the same time, Chl a concentration at the innermost and western parts of the bay increased
413 by 4–15 μg $L^{-1}$ (**Fig. S4**). Therefore, the increase of PP at the innermost part of the bay
414 was attributed to spring bloom. In contrast, PP at the southeastern part of the bay was
415 400–700 mg-C $m^{-2}$ $d^{-1}$. CDOM in the southeast was 0.06–0.12 $m^{-1}$ and low compared to
416 other areas, indicating that this part of the bay was affected by the intrusion of open-ocean
417 water derived from Kuroshio (**Fig. S3**). Since the open-ocean water was low in nutrients,

418 the PP in the southeast bay was considered to be low. In April, the spring bloom expanded
419 to the southeastern part of the bay and the PP ranged from 400–1400 mg-C $m^{-2}$ $d^{-1}$. Such
420 high productivity continued into September. In August-September, the highest PP was
421 observed at the bay (500–1600 < mg-C $m^{-2}$ $d^{-1}$) due to terriegeneous load, which agreed
422 well with the high CDOM (**Figs. S5 and S6**). In October, PP of the bay decreased to 400–
423 1200 mg-C $m^{-2}$ $d^{-1}$. From November to December, PP at the bay decreased further to 250–
424 700 mg-C $m^{-2}$ $d^{-1}$ except for blooming areas.
425
426 **3.2.2 Primary production in 2016 (Fig. 7)**
427 The low PP continued from November 2015 through January 2016. In February, spring
428 bloom (Chl a concentration 15–50< μg $L^{-1}$ **: Fig. S7**) was significantly observed at the
429 southwest coast of the bay. The spring bloom might have been triggered by terrigeneous
430 loads from the Oze and Nishiki rivers. Therefore, this bloom increased the PP to 800–
431 1600 mg-C $m^{-2}$ $d^{-1}$ at the southwest coast. The increase of PP attributed to the spring
432 bloom spread throughout the bay in March. The PP then decreased to 600–700 mg-C $m^{-2}$
433 $d^{-1}$ in April-May. However, the PP of the innermost and western parts of the bay kept 800-
434 1600 mg-C $m^{-2}$ $d^{-1}$ due to terrigeneous nutrients load from the Ohta, Oze and Nishiki rivers.
435 In June, PP at the innermost part of the bay increased again to 1600< mg-C $m^{-2}$ $d^{-1}$. This

436 increase was considered to be a result of rainfall increasing the terrigeneous load, and was
437 in good accord with high CDOM (0.20–0.24 $m^{-1}$; **Fig. S8**). This high productivity at the
438 innermost part of the bay continued into August. In September, the PP decreased due to
439 the depletion of nutrients at the center and southern parts of the bay (400–700 mg-C $m^{-2}$
440 $d^{-1}$). It is clear that the depletion of nutrients decreased the Chl a concentration to 1.8–5
441 μg $L^{-1}$ at the center and southern parts of the bay (**Fig. S9**).

442 In October, PP of the bay increased again to 600-1600 mg-C $m^{-2}$ $d^{-1}$. The high PP was
443 observed due to spring bloom at the innermost and center parts of the bay (1100-1600<
444 mg-C $m^{-2}$ $d^{-1}$). From November-December, PP of the bay decreased to 400–700 mg-C $m^{-2}$ $d^{-1}$ except for the innermost and center parts of the bay. The high PP due to autumn boom
446 partially continued at the innermost and center parts of the bay (700–1600 mg-C $m^{-2}$ $d^{-1}$).
447

448 **3.2.3 Primary production in 2017 (Fig. 8)**

449 In January-March, low-PP was observed throughout the bay, ranging from 150–800
450 mg-C $m^{-2}$ $d^{-1}$. In April, PP at the innermost and western cost of the bay increased to 400–
451 1400 mg-C $m^{-2}$ $d^{-1}$ due to spring bloom. In May, PP at innermost of the bay reached to
452 700-1600 mg-C $m^{-2}$ $d^{-1}$. In July-August, high PP was observed throughout the bay, 900–
453 1600< mg-C $m^{-2}$ $d^{-1}$ and 600–1000 mg-C $m^{-2}$ $d^{-1}$ for the innermost area and central to

454 southern areas, respectively. The high PP was considered to be due to the supply of
455 nutrients from terrigeneous and vertical mixing caused by a typhoon. The high PP slightly
456 decreased in September-October, which might have been due to nutrient depletion after
457 the bloom. In November-December, the low-PP area (150–400 mg-C $m^{-2}$ $d^{-1}$) expanded
458 throughout the bay.
459
460 **3.2.4 Summary of the PP in Hiroshima Bay**
461 In January, the PP in Hiroshima Bay ranged <50-1000 mg-C $m^{-1}$ $d^{-1}$ (**Figs. 6, 7 and 8**).
462 In spring, increases in seasonal irradiance create favorable conditions for phytoplankton
463 growth (Dugdale et al., 2007). Just like, Solent, estuary system on the south coast of the
464 UK (Iriarte and Purdie, 2004) and San Francisco Bay, USA (Dugdale, 2007), spring
465 bloom was observed at the innermost and western parts of the Hiroshima Bay. In February
466 to March 2015 and February 2016, high chlorophyll concentration (10-50< μg $L^{-1}$)
467 observed at the innermost and western parts of the bay (ex. **Figs. S4 and S7**) and the PP
468 increased to 700-1600 mg-C $m^{-1}$ $d^{-1}$ at the innermost and western parts of the bay (**Fig. 6**
469 **and 7**) substantially affected by terrigeneous load from the Ohta (2.82 x 106 $m^3$ $d^{-1}$), Oze
470 (7.99 x 105 $m^3$ $d^{-1}$) and Nishiki (1.06 x 106 $m^3$ $d^{-1}$) rivers (Lee and Hoshika, 2000). The
471 observed concentrations of DIN, DIP and DSi at surface seawater ranged 2.5-18.1 μmol

472 $L^{-1}$, 0.5-1.0 μmol $L^{-1}$ and 11.8-41.5 μmol $L^{-1}$, respectively at the innermost and western
473 parts of the bay in February 2015. Therefore, the primary nutrients supplied from
474 terrigeneous load and estuary circulation were sufficient for growth of phytoplankton.
475 The beginning of PP increase due to spring bloom was April in 2017, and it was 1-2 month
476 later compared to that in 2015 and 2016 (**Figs. 6, 7 and 8**). The SST is also one of factors
477 in controlling spring bloom. When a wind velocity (especially north wind) exceeds 10 m
478 $s^{-1}$, wind energy produces turbulence in the surface water and tends to deform the
479 stratification in northern Hiroshima Bay (Hashimoto et al., 2000). Most of daily
480 maximum wind velocity (north–south component) was less than 10 m $s^{-1}$ at the innermost
481 Hiroshima Bay (Yamamoto et al., 2002). Therefore, surface mixing layer might become
482 shallow and SST increase to favorable conditions for phytoplankton growth in March.
483 The SST at spring bloom observed area in March 2015, 2016 and 2017 increased to 11-
484 14 ºC, 11-14 ºC, and 9-12 ºC, respectively (**Fig. S10, S11 and S12**). The SST in March
485 2017 was low compared to that in 2015 and 2016. Hence, the delay of spring bloom in
486 2017 attributed to low sea surface water temperature.

487 After the spring bloom, the highest PP was observed in June- July 2016 (1600<. mg-C
488 $m^{-2}$ $d^{-1}$). Monthly rainfall in June 2015, 2016 and 2017 at Hiroshima Prefecture were
489 237.5 mm, 509.5 mm and 261.0 mm, respectively (Japan Metrological Agency). The

490 rainfall in June 2016 was twice of that in 2015 and 2017, suggesting that high terrigeneous
491 loads which could be supposed by the fact that the CDOM (0.22-0.24 $m^{-1}$) was high at
492 the innermost of the bay in June 2016 compared to 2015 and 2017 (**Figs. S8, S13 and**
493 **S14**). Yamamoto et al, 2011 reported that estuary circulation increased when the
494 increasing flow rate of Ohta river. Therefore, both terrigeneous load and upwelling of
495 nutrients due to increasing in estuary circulation kept PP high at the innermost of the bay
496 in June 2016 (**Fig. 7**). The high productivity continued into September at the innermost
497 of the bay. In summer, hypoxic water mass is observed at the innermost of the bay every
498 year (Yamamoto et al, 2011; Asaoka et al., 2018). Under such anoxic condition, nutrients
499 especially phosphate adsorbed on organically enriched sediments desorbe in water
500 column. Hence, nutrients dissolution from sediments as well as terrigeneous load might
501 increase PP at the innermost of the bay.

502 In autumn, although haloclines were slightly observed due to fresh water inflow from
503 the Ota River at the innermost of the bay, the vertical mixing of seawater resulted in the
504 disappearance of haloclines (Asaoka et al., 2018). Autumn bloom was partially observed
505 at the innermost and center parts of the bay. The PP in November to December ranged
506 150-600 mg-C $m^{-2}$ $d^{-1}$ except for blooming areas (**Figs. 6,7 and 8**).

507

## 4. Conclusions

We estimated the PP in Hiroshima Bay, Japan with a modified Kameda & Ishizaka model using an OCS, GOCI-COMS. Our proposed method is superior to previous methods for estimating PP in coastal seas due to its higher temporal and spatial resolution. The coefficient of determination between observed and estimated PP by the OCS was $r^2$=0.750. The slope of the linear regression was 1.00. The RMSE was 165 mg-C $m^2$ $d^{-1}$, which is sufficient for discussions of changes in spatial distribution of Hiroshima Bay. We underscore line that our proposed method based on the high-resolution (approx. 500 m) ocean-color product can estimate ocean primary production in coastal seas including complicated topographic areas such as enclosed seas or channels less than 1 km wide where the conventional method cannot be employed applied.

## Acknowledgements

This study was partially supported by a grant from the Environment Research and Technology Development Fund (S-13) of the MOE, Japan (S-13), the promotional grant for multi-disciplinary concept from young researchers, Kobe University, and the joint research program of the Institute for Space-Earth Environmental Research (ISEE), Nagoya University. The authors would like to thank Dr. Sosuke Otani, Osaka Prefecture

University College of Technology, Dr. Naoki Fujii, Saga University, and Dr. Kotaro Hirose, Waseda University for their help with sampling and thoughtful suggestions. The authors are grateful to the captain and crew of the research & training vessel, Toyoshio-Maru, Hiroshima University, and the training vessel, Hikari, National Institute of Technology, Hiroshima College, for their navigation.

## References

Amin, R., Gould, R., Ladner, S., Shulman, L., Jolliff, J., Sakalaukus, P., Lawson, A., Martinolich, P., Arnone, R.2013. Inter-Sensor Comparison of Satellite Ocean Color Products from GOCI and MODIS. AMS Proceedings, pp5.

Arrigo, K.R., Dijken, G.L. 2011. Secular trends in Arctic Ocean net primary production. J. Geophys. Res. 116, C09011

Asaoka, S., Umehara, A., Otani, S., Fujii, N., Okuda, T., Nakai, S., Nishijima, W., Takeuchi, K., Shibata, H., Jadoon, W. A., Hayakawa, S. 2018. Spatial distribution of hydrogen sulfide and sulfur species in coastal marine sediments Hiroshima Bay, Japan. Mar. Pollut. Bull. 133, 891-899.

Bauer, J.E., Cai, W.J., Raymond, P.A., Bianchi, T.S., Hopkinson, C.S., Regnier, P.A.G. 2013.The changing carbon cycle of the coastal ocean. Nature 504, 61-70.

544 Behrenfeld, M. J., Falkowski, P. G., 1997. Photosynthetic rates derived from satellite-
545 based chlorophyll concentration. Limnol. Oceanogr., 42(1), 1-20.
546 Behrenfeld, M. J., O'Malley, R. T., Siegel, D. A., McClain, C. R., Sarmiento, J. L.,
547 Feldman, G. C., Milligan, A. J., Falkowski, P. G., Letelier, R. M., Boss, E. S. 2006.
548 Climate-driven trends in contemporary ocean productivity. Nature, 444, 752-755.
549 Bosc, E., Bricaud, A., Antoine, D. 2004. Seasonal and interannual variability in algal
550 biomass and primary production in the Mediterranean Sea, as derived from 4 years
551 of SeaWiFS observations. Glob. Biogeochem. Cycles, 18, GB1005.
552 Choi, J.K., Park, Y.J., Ahn, J.H., Lim, H.S., Eom, J., Ryu, J.H. 2012. GOCI, the world's
553 first geostationary ocean color observation satellite, for the monitoring of temporal
554 variability in coastal water turbidity. J. Geophys. Res. 117(C9), 1-10.
555 Cota, G.F., Harrison, W.G., Platt, T., Sathyendranath, S. Stuart, V. 2003. Bio-optical
556 properties of the Labrador Sea. J. Geophys. Res. 108(C7), 1-14.
557 Dugdale, R.C., Wilkerson, F.P., Hogue, V.E., Marchi, A. 2007. The role of ammonium
558 and nitrate in spring bloom development in San Francisco Bay. Estuar., Coast. Shelf
559 Sci. 73(1-2), 17-29.
560 Engel, A., Borchard, C., Piontek, J., Schulz, K., Riebesell, U., Bellerby, R. 2013. $CO_2$
561 increases $^{14}C$ primary production in an Arctic plankton community. Biogeosci. 10(3),

562 1291-1308.

563 Falkowski,P.G., Barber, R.T., Smetacek, V. 1998. Biogeochemical controls and
564 feedbacks on ocean primary production. Science 281(5374), 200-206.

565 Feldman, G., Kuring, N., Ng, C., Esaias, W., McClain, C., Elrod, J., Maynard, N., Endres,
566 D., Evans, R., Brown, J., Walsh, S., Carle, K., Podesta, G. 1989. Ocean color:
567 Availability of the global data set. EOS, 70(23), 634-641.

568 Friedland, K.D., Stock, C., Drinkwater, K. F., Link, J.S., Leaf, R.T., Shank, B.V., Rose,
569 J.M., Pilskaln, C.H., Fogarty M.J. 2012. Pathways between primary production and
570 fisheries yields of large marine ecosystems. PLOS ONE 7(1)e28945. doi
571 10.1371/journal.pone.0028945

572 Gaarder, T., Gran, H. H. 1927. Investigations of the production of plankton in the Oslo
573 Fjord. Rapports et procès-verbaux des réunions / Conseil permanent international
574 pour l'exploration de la mer. 42, 1-48.

575 Gordon, H.R. 1997. Atmospheric correction of ocean color imagery in the Earth
576 Observing System era. J. Geophys. Res. 102(D14), 17081-17106.

577 Hama, T., Miyazaki, T., Ogawa, Y., Iwakuma, T., Takahashi, M., Otsuki A., Ichimura
578 S.1983. Measurement of photosynthetic production of a marine phytoplankton
579 population by using a stable $^{13}C$ isotope. Marine Biol. 73(1),31-36.

580 Hashimoto, E., Zhu, X.-H., Nagao, M., Takasugi, Y., 2000. Influence of wind on estuarial
581 condition in the Hiroshima Bay. Umi to Sora 76(3), 137-143 (in Japanese with
582 English abstract).
583 Hayashi, M., Ishizaka, J., Kobayashi, H., Toratani, M., Nakamura, T., Nakashima, Y.,
584 Yamada, S. 2015. Evaluation and improvement of MODIS and SeaWIFS-derived
585 Chlorophyll a concentration in Ise-Mikawa Bay. J. Remote Sensing Soc. Japan 35(4),
586 245-259.(in Japanese with English abstract)
587 Iriarte, A., Purdie, D.A. 2004. Factors controlling the timing of major spring bloom
588 events in an UK south coast estuary. Estuar., Coast. Shelf Sci. 61(4), 679-690.
589 Japan Metrological Agency, http://www. data. jma. go. jp/obd/stats/etrn/index.php?
590 prec_no=67&block_no=47765&year=2017&month=&day=&view=p1
591 Japan River Association, http://www.japanriver.or.jp/
592 Johanna, A. L., Goldman, Sven, A K., Jodi N.Y., Philippe, D.T., Rachel, H.R., S,
593 Michael, .L. B., Francois M. M. M. 2015. Gross and net production during the spring
594 bloom along the Western Antarctic Peninsula. New Phytologist 205(1)182-191.
595 Kameda, T., Ishizaka J. 2005. Size-fractionated primary production estimated by a two-
596 phytoplankton community model applicable to ocean color remote sensing. J.
597 Oceanogr. 61(4), 663-672.

598 Kluijver, A., Soetaert, K., Czerny, J., Schulz, K. G., Boxhammer, T., Riebesell, U.,
599 Middelburg, J.J. 2013. A $^{13}C$ labelling study on carbon fluxes in Arctic plankton
600 communities under elevated $CO_2$ levels. Biogeosci. 10(3), 1425-1440.
601 Korea Ocean Satellite Center (http://kosc.kiost.ac/eng/p20/kosc_p21.html)
602 Lee, I.C., Hoshika, A. 2000. Seasonal variations in pollutant loads and water quality in
603 Hiroshima Bay. J. Japan Soc. Water Environ. 23(6), 367-373 (in Japanese with
604 English abstract).
605 Lyngsgaard, M.M., Richardson, K., Markager, S., Nielsen, M.H., Olesen, M.,
606 Christensen, J.P.A. 2014. Deep primary production in coastal pelagic systems:
607 importance for ecosystem functioning. Marine Ecol. Progress Ser. 517, 15-33.
608 Nakada, S., Kobayashi, S., Hayashi, M., Ishizaka, J., Akiyama, S., Fuchi, M., Nakajima,
609 M. 2018. High-resolution surface salinity maps in coastal oceans based on
610 geostationary ocean color images: quantitative analysis of river plume dynamics. J.
611 Oceanogr., 74, 287-304
612 Platt, T. , Sathyendranath, S., 1988. Oceanic primary production: estimation by remote
613 sensing at local and regional scales. Science, 241(4873), 1613-1620.
614 Ryu, J.H., Han, H.J., Cho, S., Park, Y.J., Ahn, Y.H. 2012. Overview of geostationary
615 ocean color imager (GOCI) and GOCI data processing system (GDPS). Ocean Sci.

616 J. 47(3), 223-233.
617 Saino, T. 1993. Satellite ocean color remote sensing and primary productivity in the
618 ocean. Bull. Coast. Oceanogr. 31(1), 129-152. (in Japanese with English abstract)
619 Sasaki, H., Siswanto, E., Nishiuchi, K., Tanaka, K., Hasegawa, T., Ishizaka, J. 2008.
620 Mapping the low salinity Changjiang Diluted Water using satellite-retrieved colored
621 dissolved organic matter (CDOM) in the East China Sea during high river flow
622 season. Geophys. Res. Letters 35(4): L04604, doi:10.1029/2007GL032637
623 Shiozaki,T., Kodama, T., Kitajima, S., Sato, M., Furuya, K. 2013. Advective transport
624 of diazotrophs and importance of their nitrogen fixation on new and primary
625 production in the western Pacific warm pool. Limnol. Oceanogr. 58(1), 49-60.
626 Siegel, D.A, Buesseler, K.O., Behrenfeld, M.J., Benitez-Nelson, C.R., Boss, E.,
627 Brzezinski, M.A., Burd, A., Carlson C.A, D'Asaro, E.A., Doney, S.C., Perry, M.J.,
628 Stanley, R.H.R. , Steinberg, D.K. 2016. Prediction of the export and fate of global
629 ocean net primary production: The EXPORTS science plan. Front. Mar. Sci. 3, 1-10.
630 Steemann Nielsen. E., 1952. The use of radioactive carbon ($^{14}C$) for measuring organic
631 production in the sea. Journal du Conseil / Conseil Permanent International pour
632 l'Exploration de la Mer 18, 117-140.
633 Tsuchiya, K., Yoshiki, T., Nakajima, R., Miyaguchi, H., Kuwahara, V. S., Taguchi, S.,

634 Kikuchi, T., Toda, T. 2013. Typhoon-driven variations in primary production and
635 phytoplankton assemblages in Sagami Bay, Japan: A case study of typhoon Mawar
636 (T0511). Plankton and Benthos Res. 8(2), 74-87.
637 Umehara, A., Asaoka, S., Fujii, N., Otani, S., Yamamoto, H., Nakai, S., Okuda, T.
638 Nishijima, W. 2018. Biological productivity evaluation at lower trophic levels with
639 intensive Pacific oyster farming of *Crassostrea gigas* in Hiroshima Bay, Japan.
640 Aquaculture, 495, 311-319.
641 Welschmeyer, N.A.1994. Fluorometric analysis of chlorophyll a in the presence of
642 chlorophyll b and pheopigments. Limnol. Oceanogr. 39(5), 1985-1992.
643 Yamamoto, T., Yoshikawa, S., Hashimoto, T., Takasugi, Y., Matsuda, O. 2000. Esuary
644 circulation process in the Northern Hiroshima Bay, Japan. Bull. Coast. Oceanograph.
645 37(2), 111-118 (in Japanese with English abstract).
646 Yamamoto, T., Hashimoto, T., Tarutani, K., Kotani, Y. 2002. Effects of winds, tides and
647 river water runoff on the formation and disappearance of the *Alexandrium tamarense*
648 bloom in Hiroshima Bay, Japan. Harmful Algae 1(3), 301-312.
649 Yamamoto, H., Yamamoto, T., Takada, T., Mito, Y., Takahashi, T. 2011. Dynamic
650 analysis of oxygen-deficient water mass formed in the northern part of Hiroshima
651 Bay using a pelagic-benthic coupled ecosystem model. J. Japan Soc. Water Environ.

652 34, 19-28 (in Japanese with English abstract).

653 Yanagi, T. (2008), Sedimentary Environments of Seto Inland Sea, 130 pp., Koseisya

654 Press, Tokyo. (in Japanese).

655

656

Figures

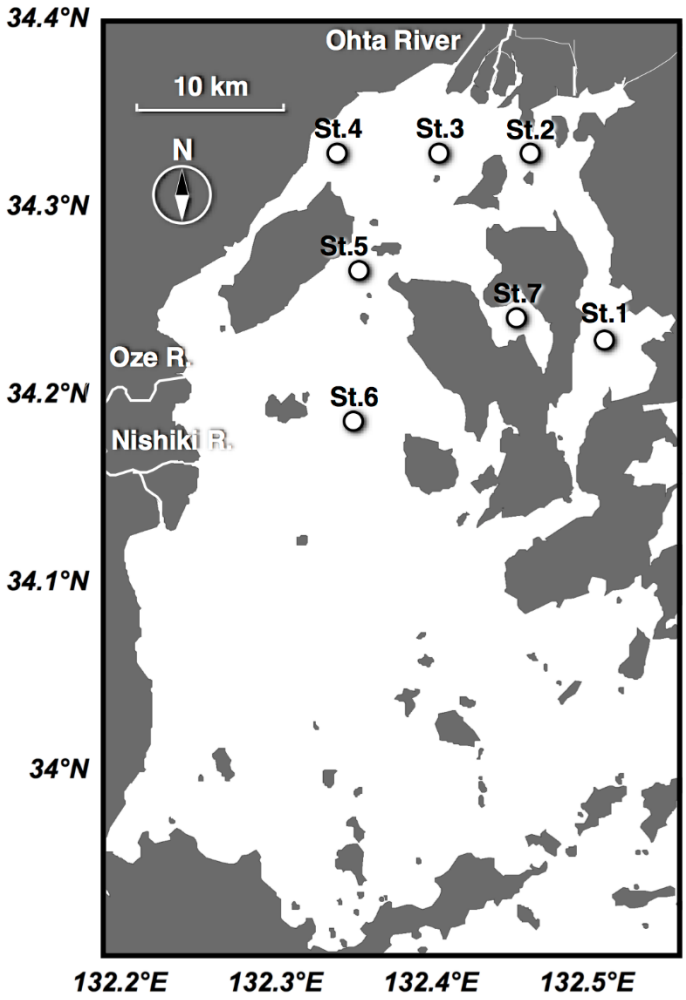


Map of sampling stations were drawn using software for the analysis and visualization of oceanographic and meteorological data sets, Ocean Data View ver. 4.7.10.

**Fig. 1Hiroshima Bay and its 7 sampling stations.**

○：seasonal sampling stations

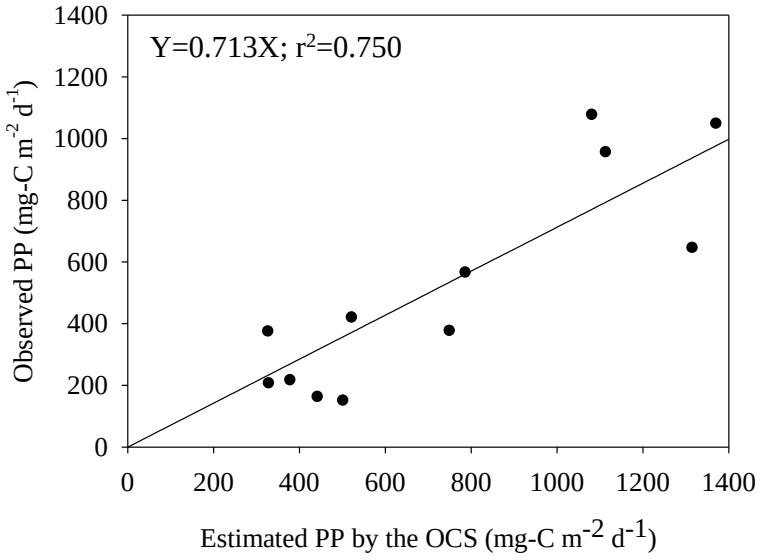


**Fig. 2 Relationship between observed and estimated PP by the OCS**

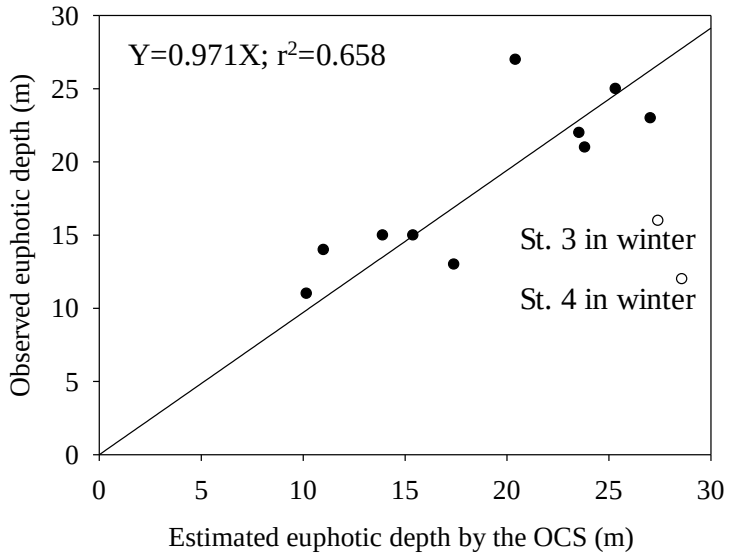


**Fig. 3 Relationship between observed and estimated euphotic depth by the OCS**

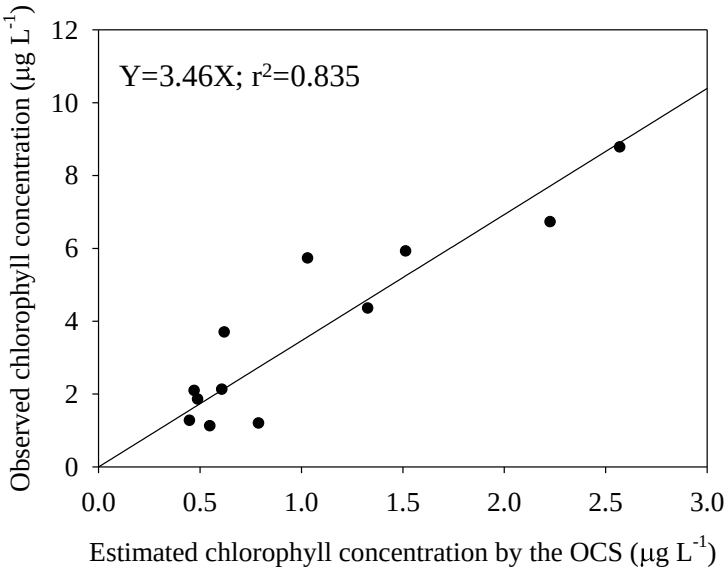


**Fig. 4 Relationship between observed and estimated chlorophyll concentration by the OCS**

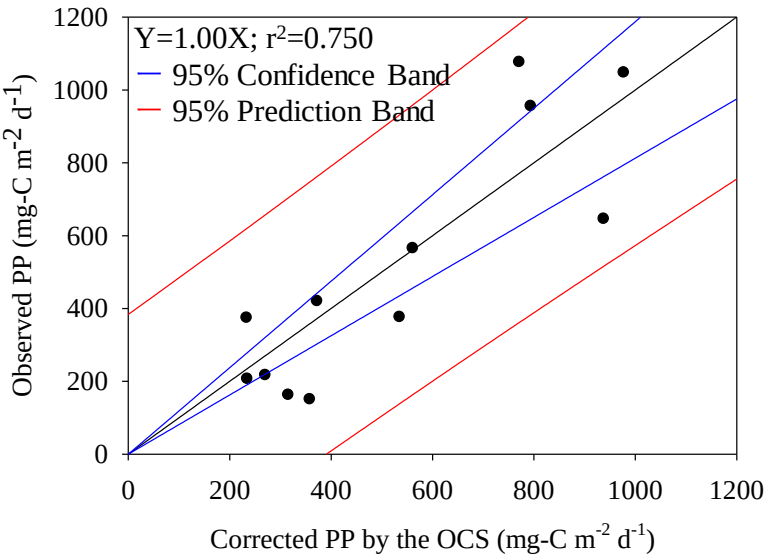


**Fig. 5 Relationship between observed and corrected PP in Hiroshima Bay estimated from the OCS**

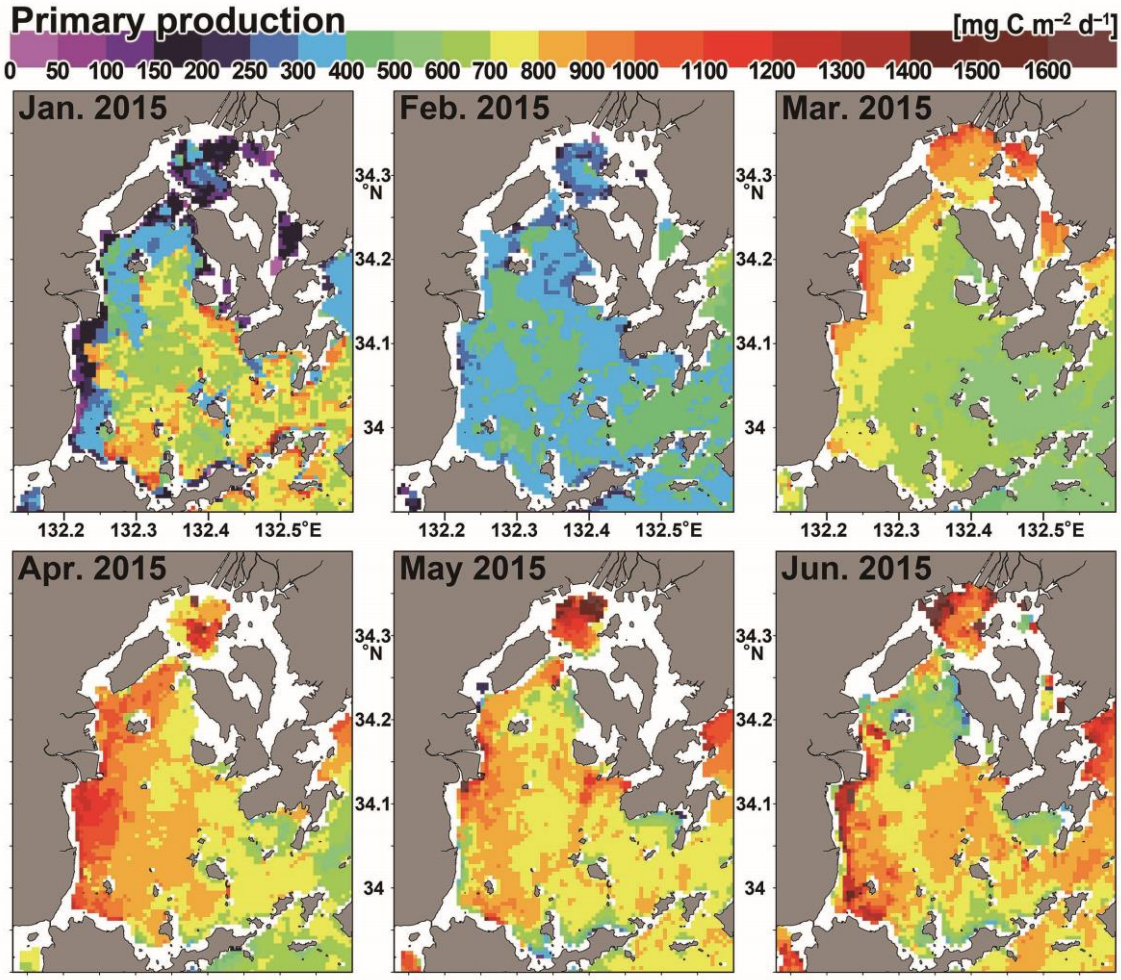


**Fig. 6 PP in Hiroshima Bay in 2015**

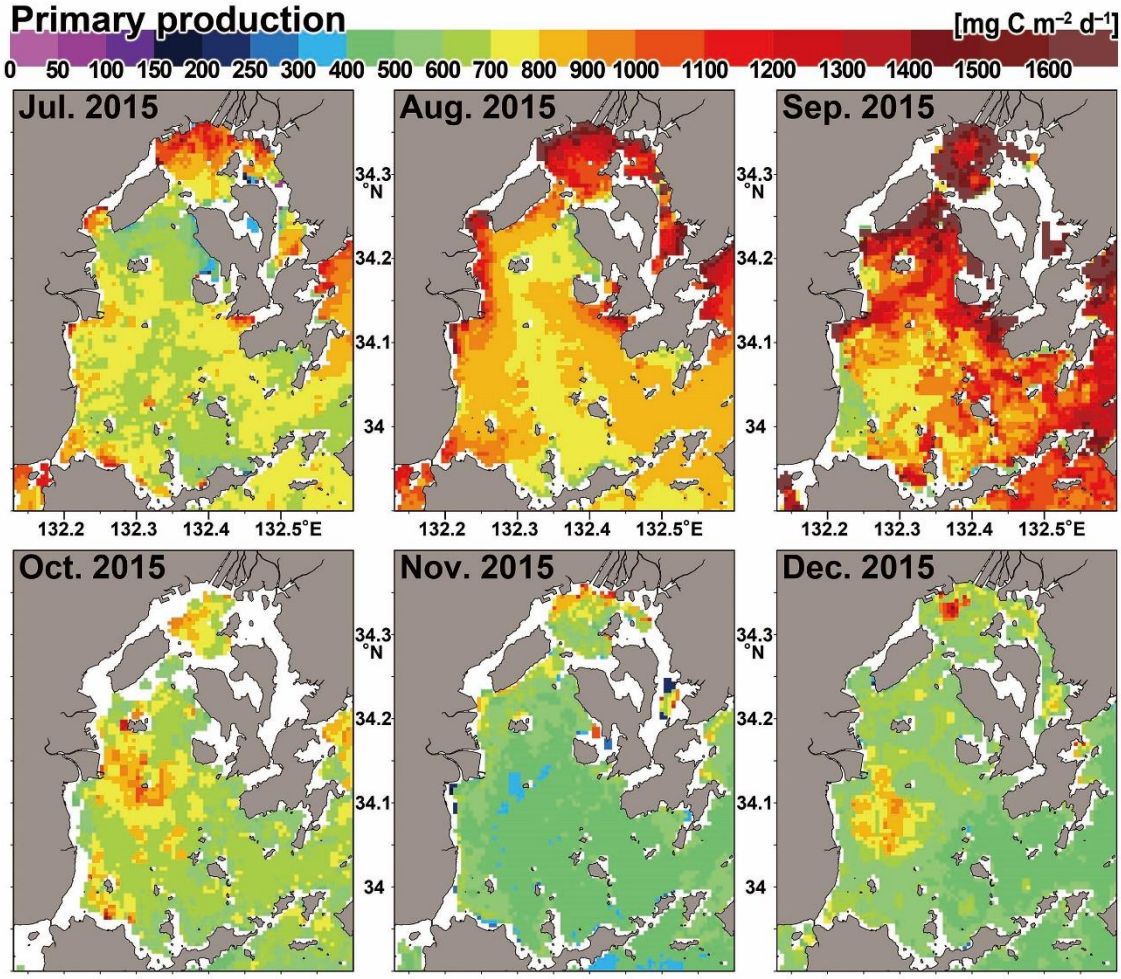


**Fig. 6 PP in Hiroshima Bay in 2015 (Continued)**

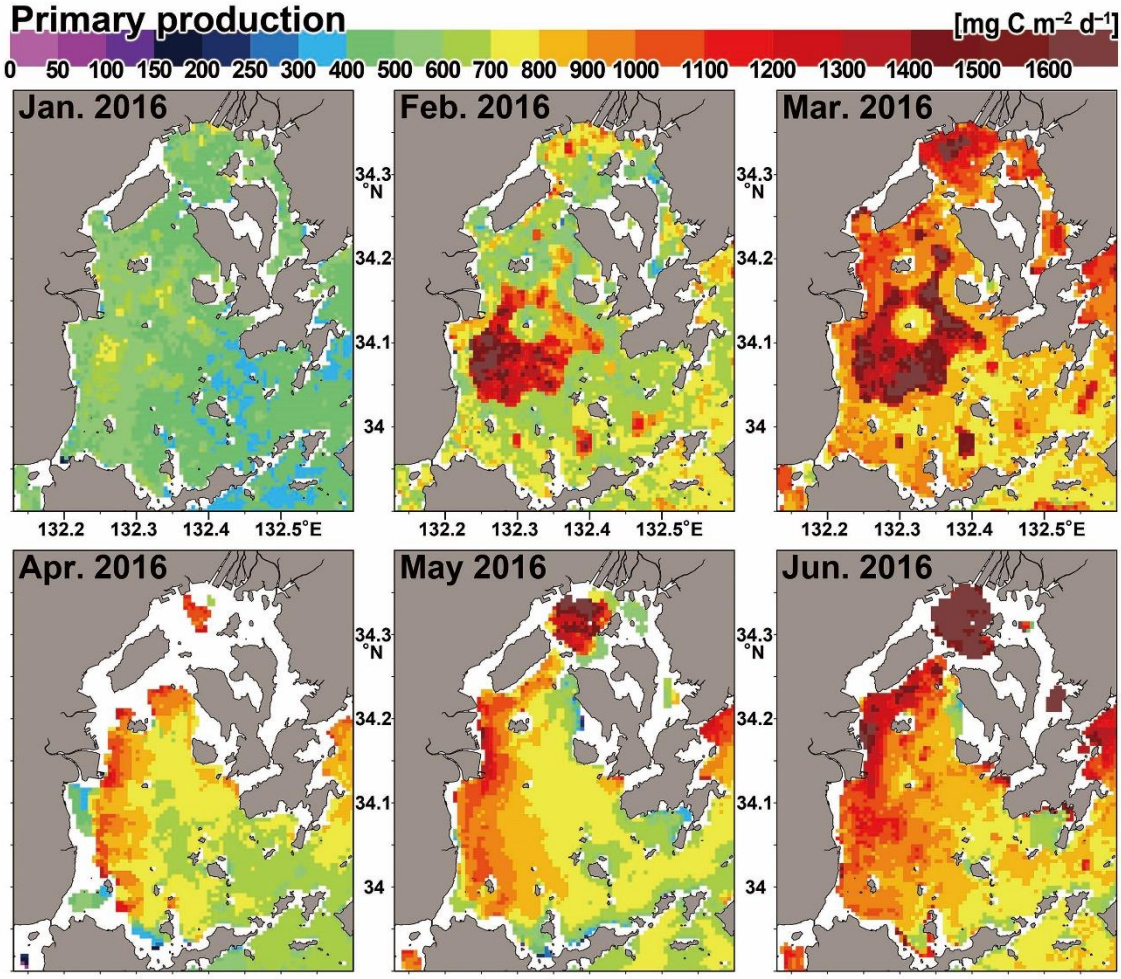


**Fig. 7 PP in Hiroshima Bay in 2016**

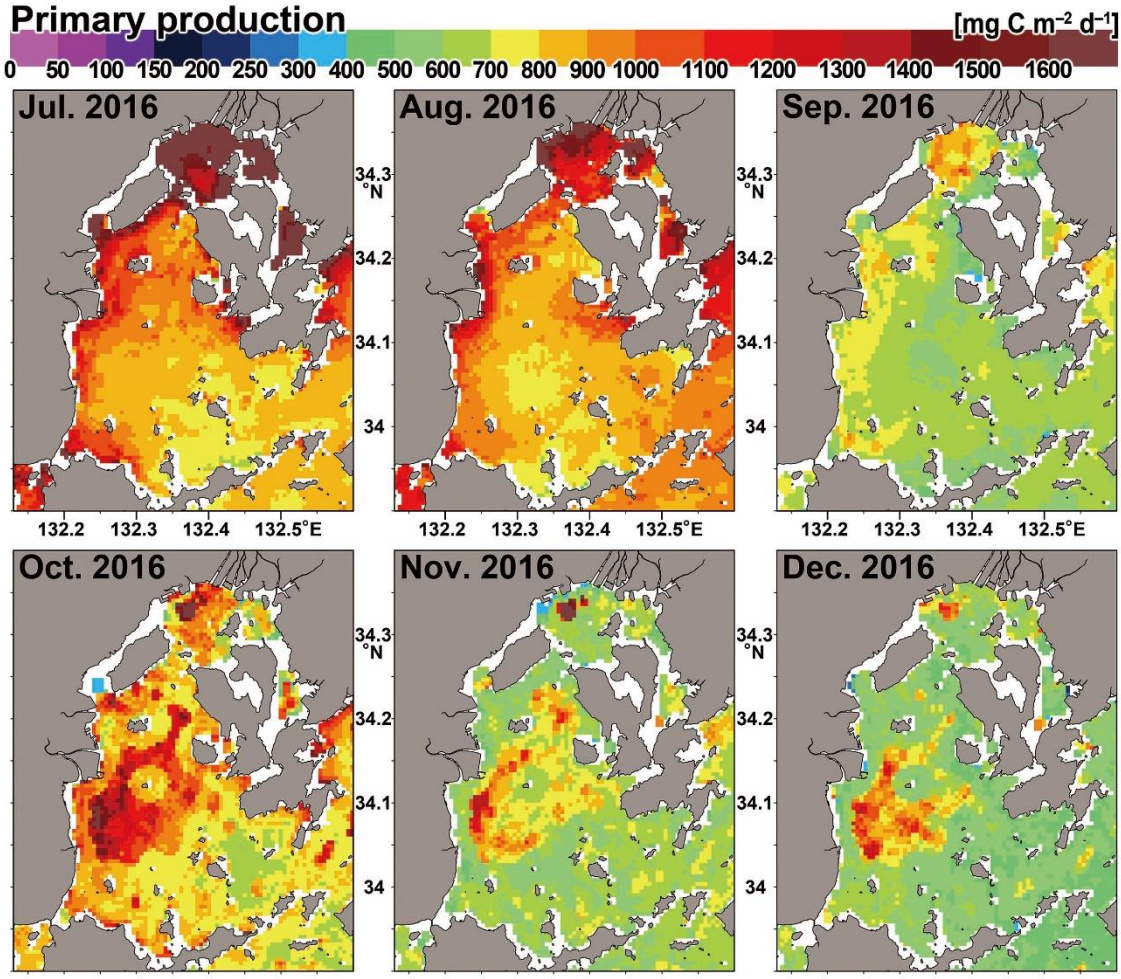


**Fig. 7 Hiroshima Bay in 2016 (Continued)**

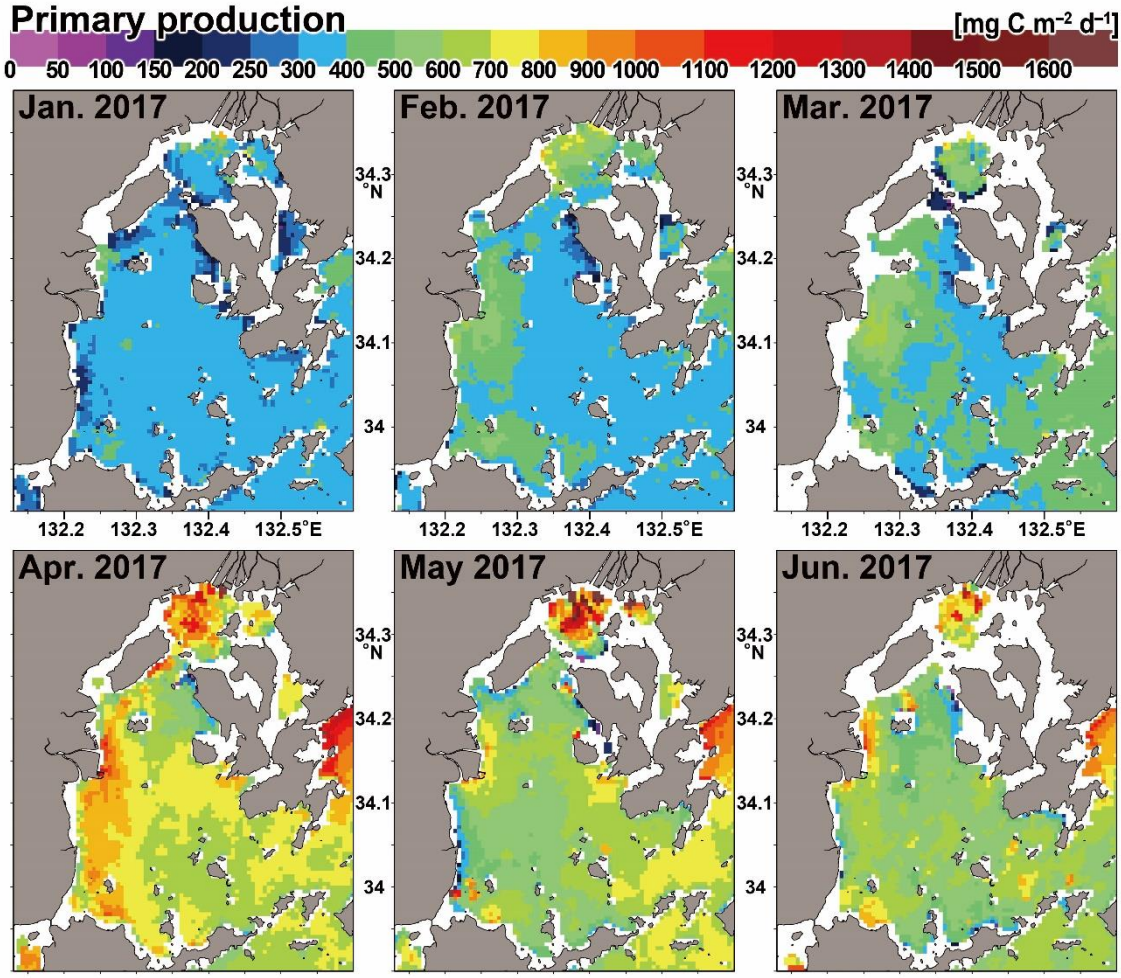


**Fig. 8 Hiroshima Bay in 2017**

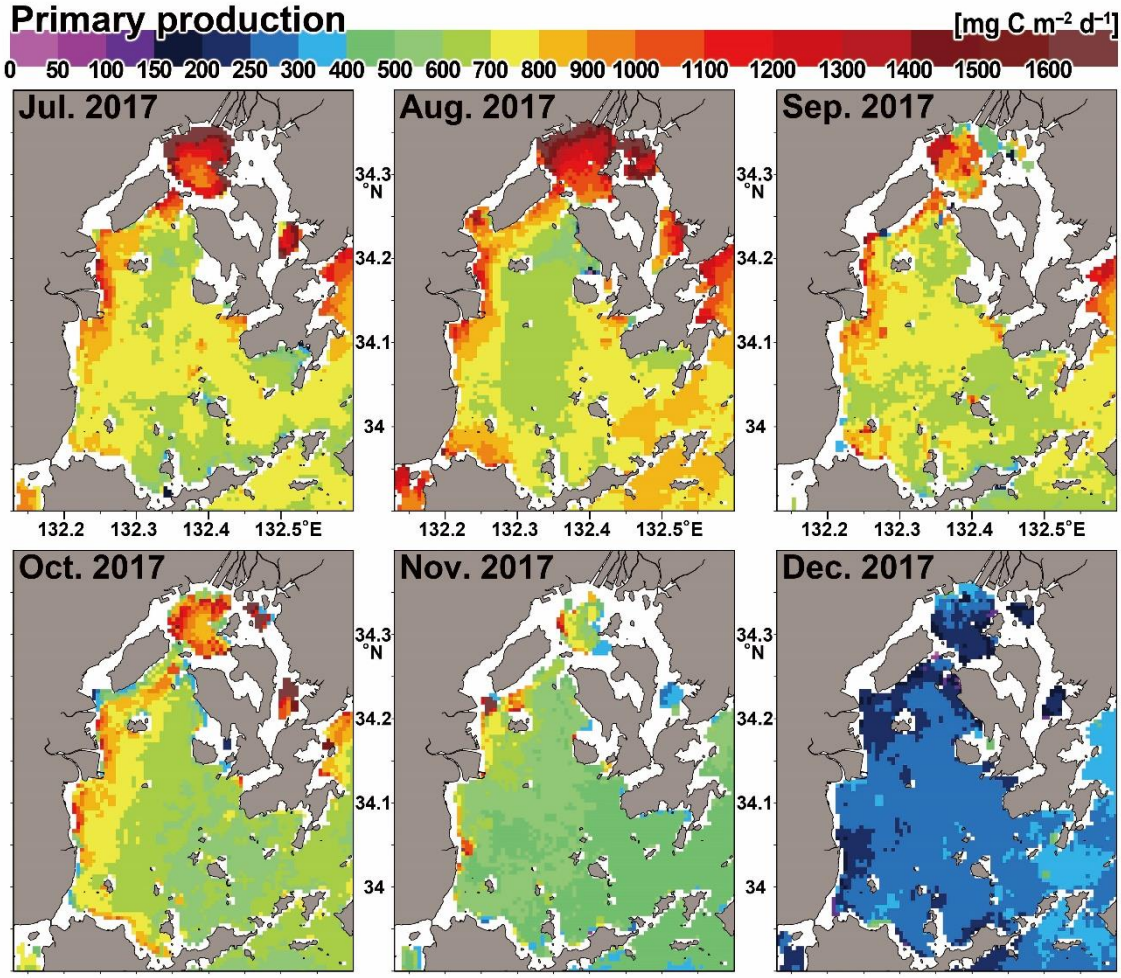


**Fig. 8 Hiroshima Bay in 2017 (Continued)**

Table 1　Comparison with the primary production estimated by the VGPMs

| Observed vs. estimated PP | This study | Behrenfeld & Falkowski (1997) | Kameda & Ishizaka (2005) |
|---|---|---|---|
| RSME | 165 | 245 | 379 |
| RMSE(%) | 31.2 | 48.6 | 122 |
| Bias | 10.8 | -14.0 | -208 |
| Slope | 1.00 | 1.08 | 1.69 |
| $r^2$ | 0.750 | 0.462 | 0.109 |

**Graphical abstract**

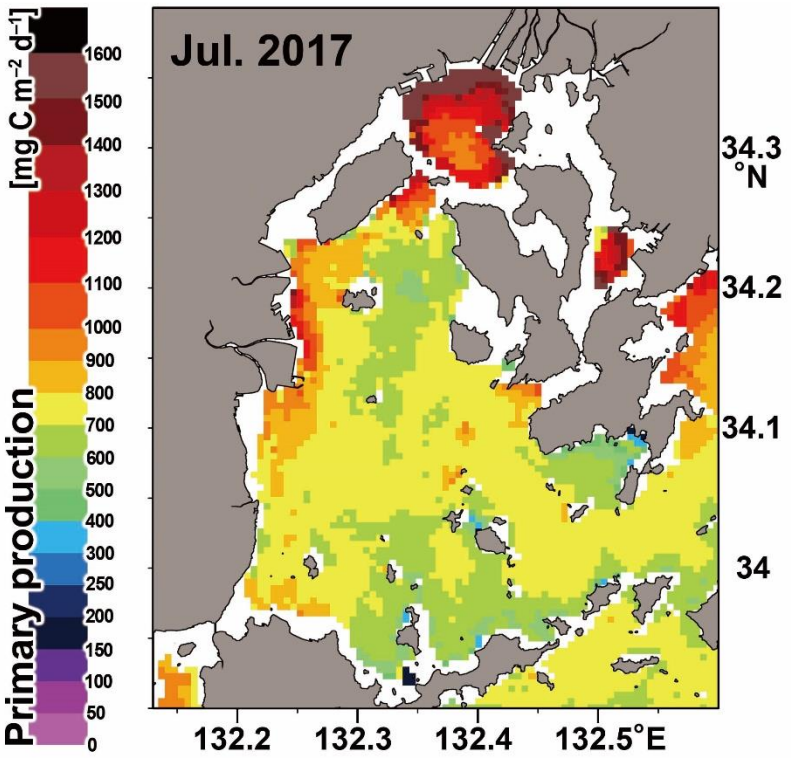


Primary production Hiroshima Bay, Japan estimated by the proposed method.

**Supplemental materials**

# Estimation of spatial distribution of coastal ocean primary production in Hiroshima Bay, Japan, with a geostationary ocean color satellite

Satoshi ASAOKA[a]*, Satoshi NAKADA[b], Akira UMEHARA[c],
Shoji ISHIZAKA[d], Wataru NISHIJIMA[c]

a Research Center for Inland Seas, Kobe University
5-1-1 Fukaeminami, Higashinada, Kobe, 658-0022 JAPAN
b Center for Regional Environmental Research, National Institute for Environmental Studies
16-2 Onogawa, Tsukuba, 305-8601 JAPAN
c Environmental Research and Management Center, Hiroshima University
1-5-3, Kagamiyama, Higashihiroshima, Hiroshima, 739-8513 JAPAN
d Institute for Space-Earth Environmental Research, Nagoya University
Furo, Chikusa, Nagoya, 464-8601 JAPAN

*Corresponding author:
Tel & Fax: +81-78-431-6357, E-mail: s-asaoka@maritime.kobe-u.ac.jp
Address: Research Center for Inland Seas, Kobe University, 5-1-1 Fukaeminami, Higashinada, Kobe, 658-0022 JAPAN

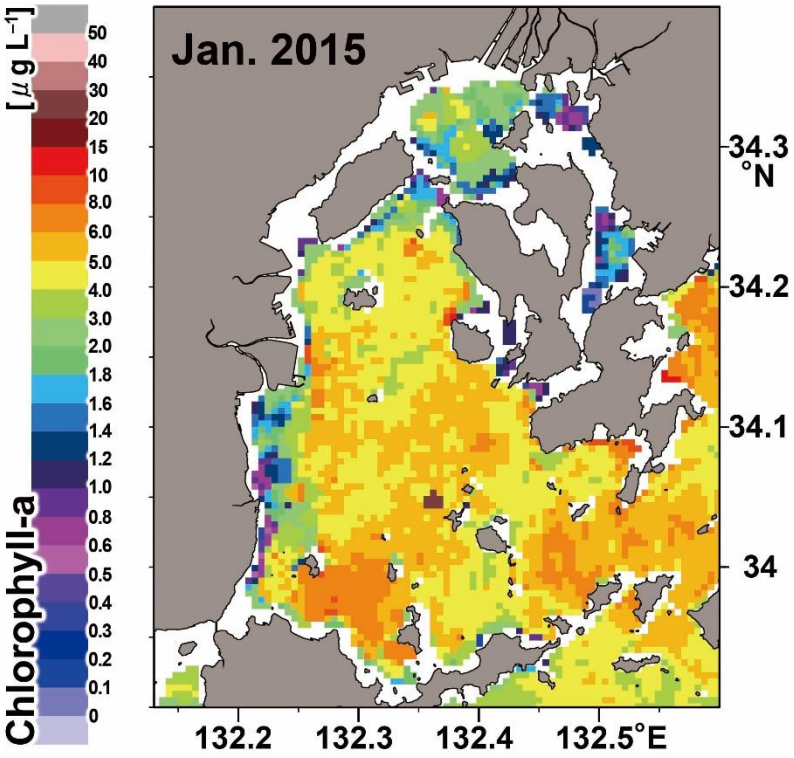


Fig. S1Chlorophyll concentration in surface seawater in January 2015

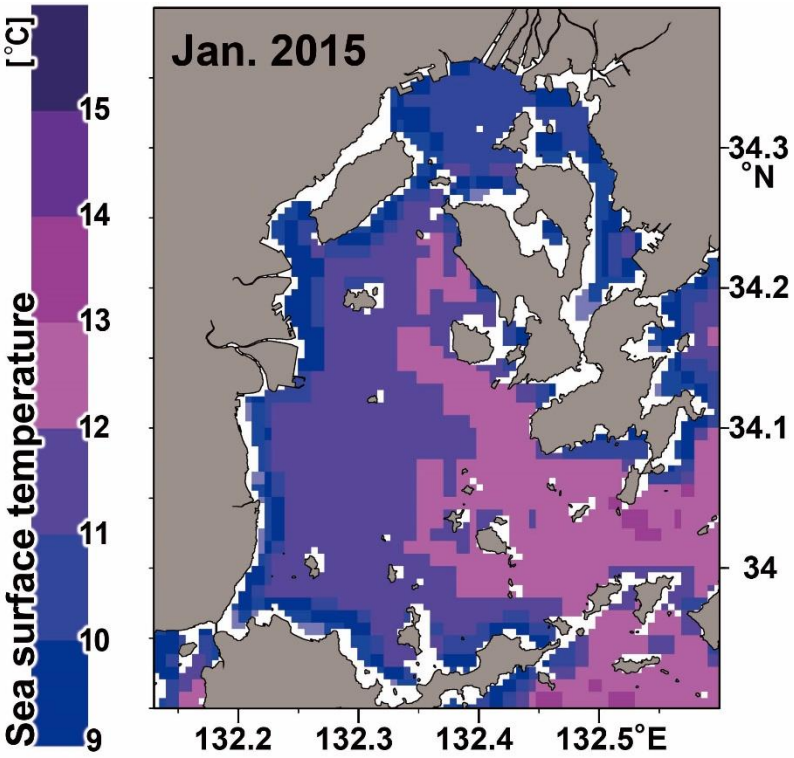


Fig. S2 Sea surface temperature in January 2015

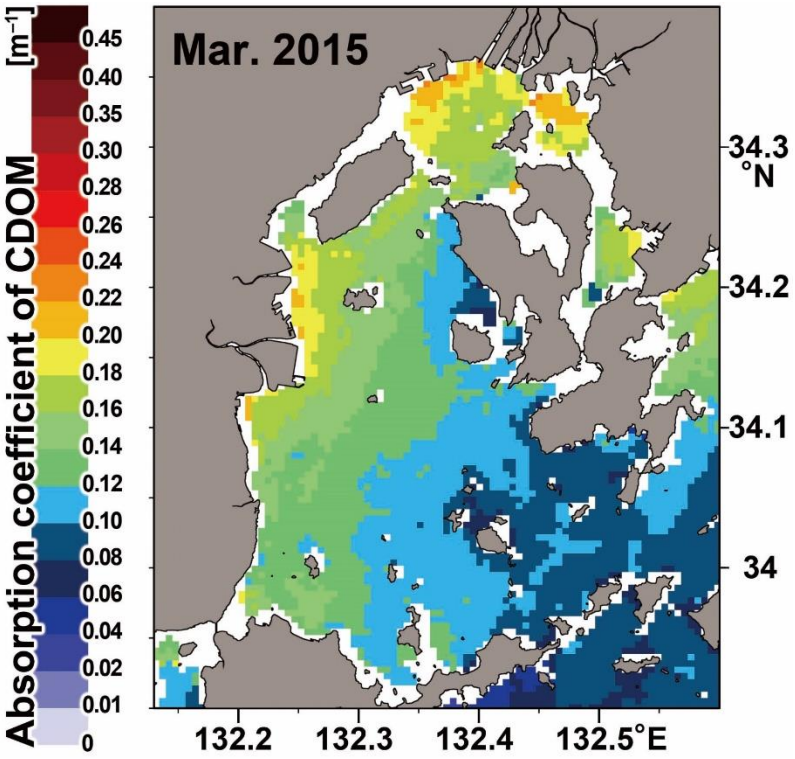


Fig. S3 CDOM in surface seawater in March 2015

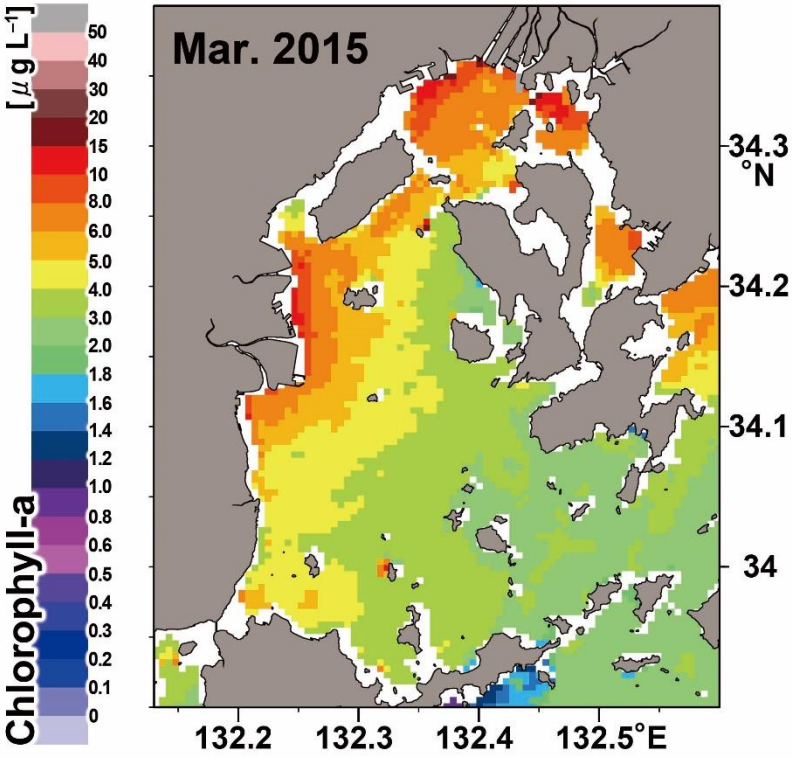


Fig. S4 Chlorophyll concentration in surface seawater in March 2015

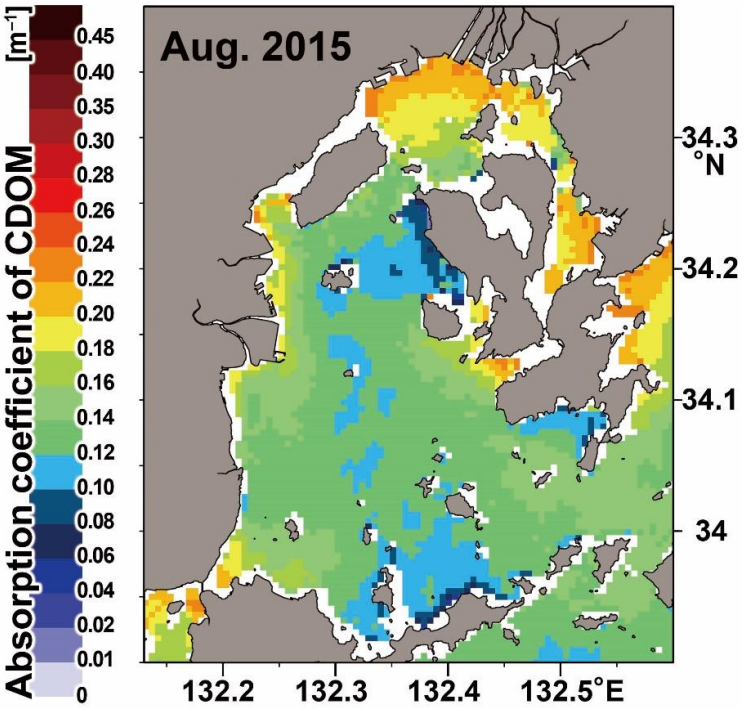


Fig.S5 CDOM in surface seawater in August 2015

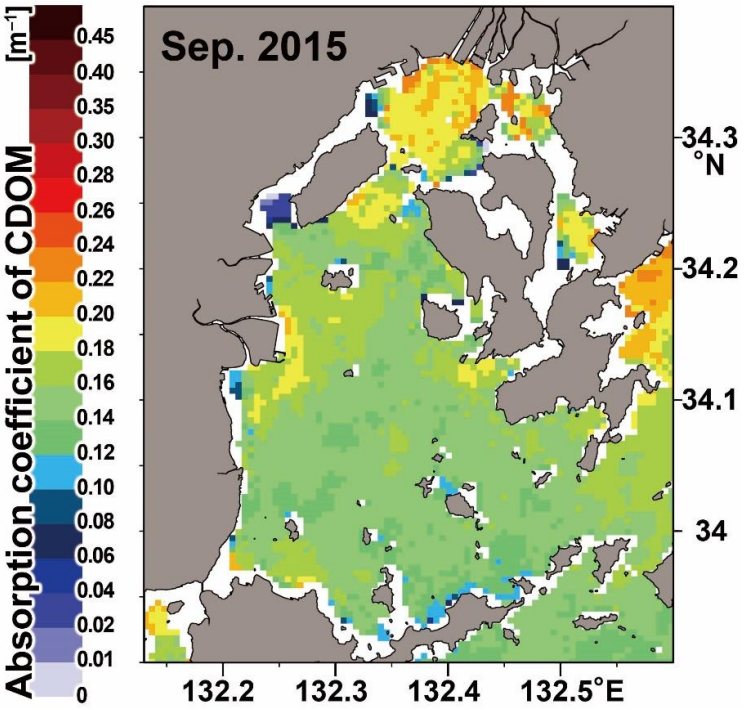


Fig. S6 CDOM in surface seawater in September 2015

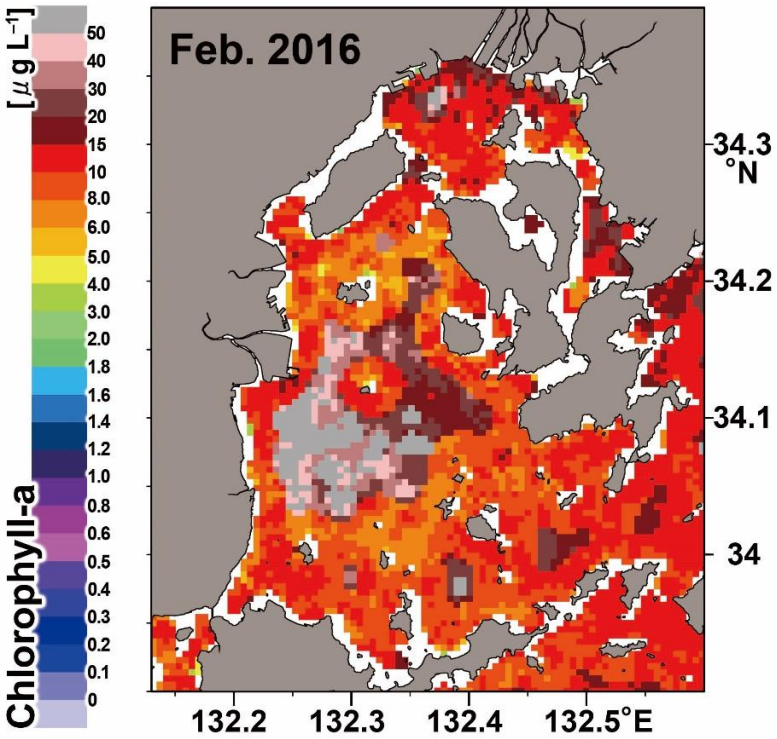


Fig. S7 Chlorophyll concentration in surface seawater in February 2016

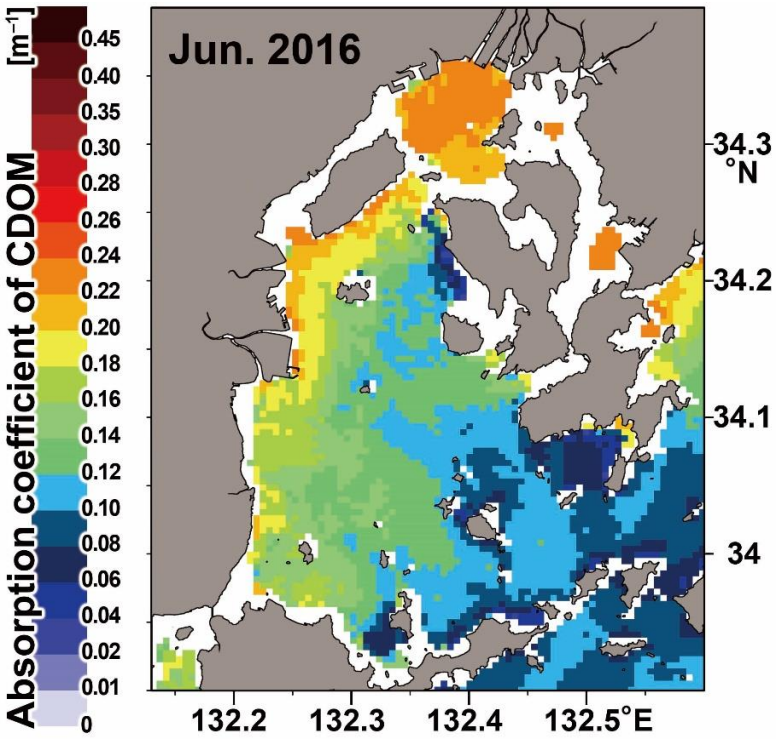


Fig. S8 CDOM in surface seawater in Jun 2016

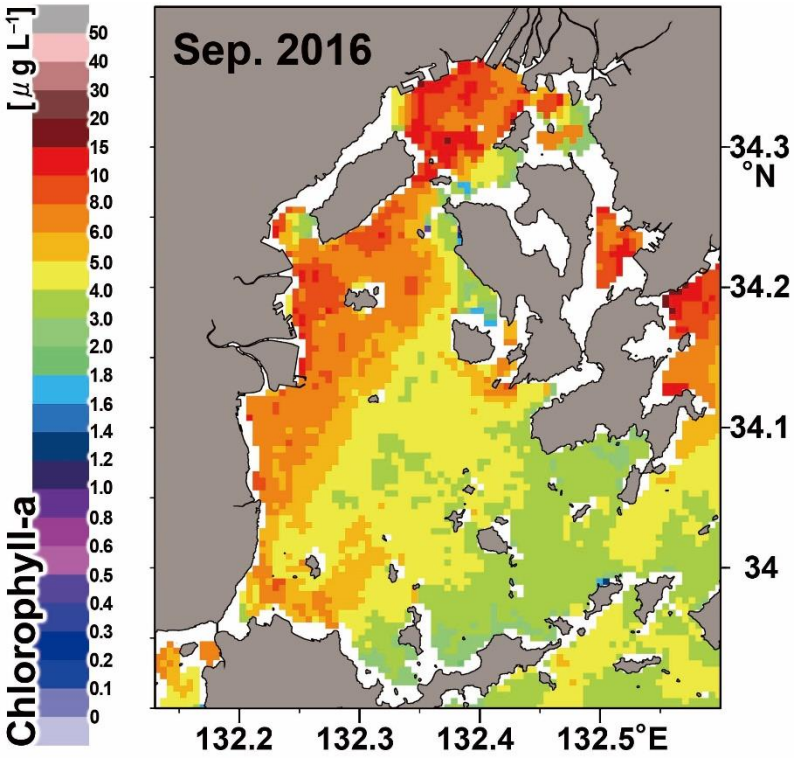


Fig. S9 Chlorophyll concentration in surface seawater in September 2016

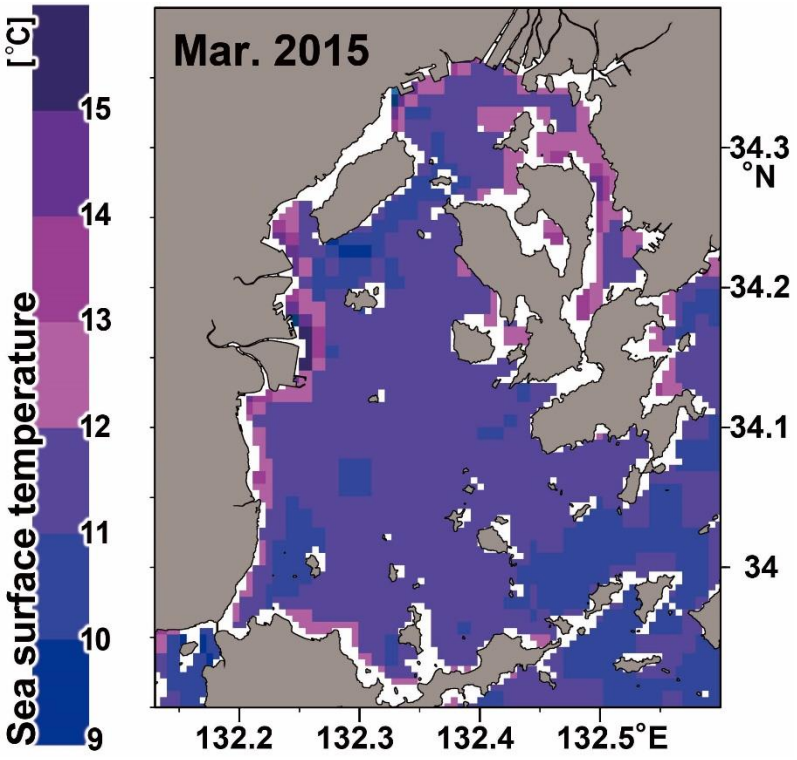


Fig. S10 Sea surface temperature in March 2015

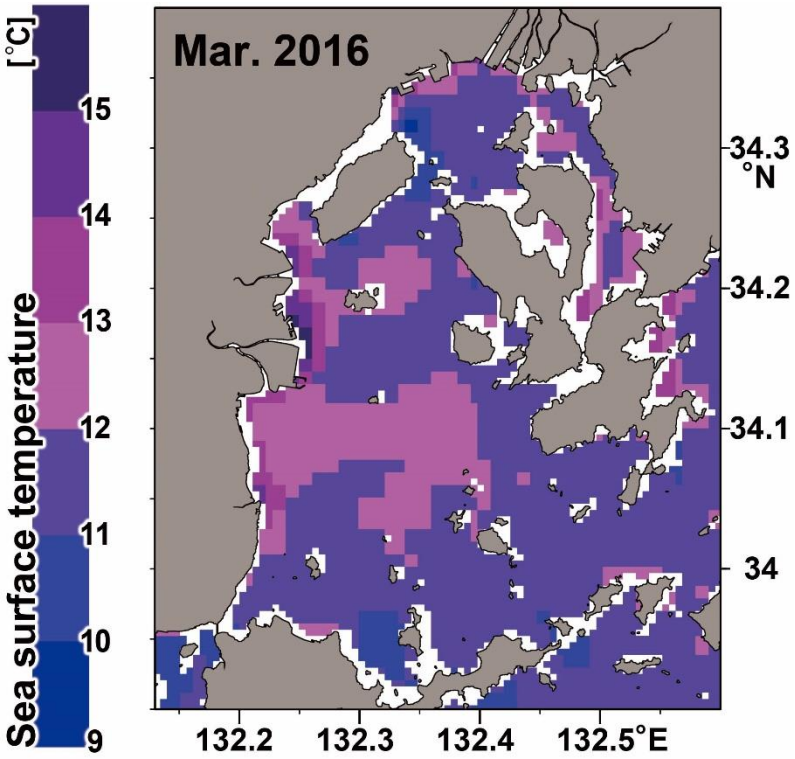


Fig. S11 Sea surface temperature in March 2016

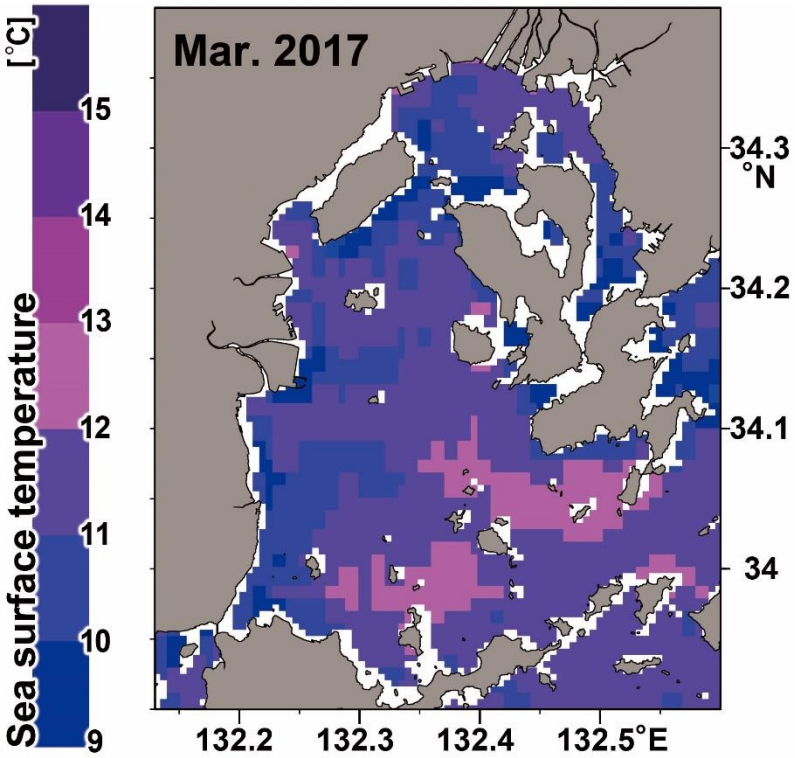


Fig. S12 Sea surface temperature in March 2017

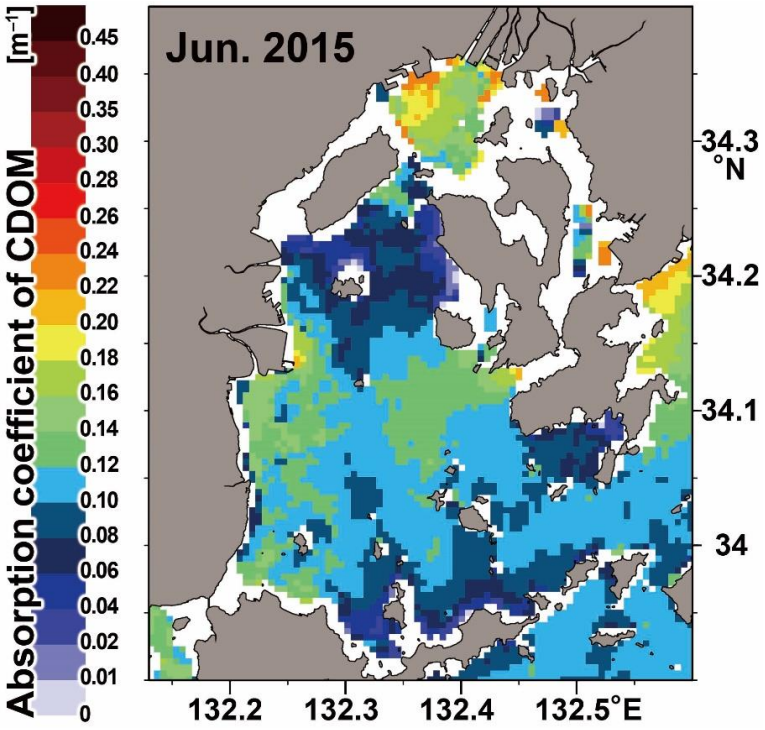


Fig. S13 CDOM in surface seawater in Jun 2015

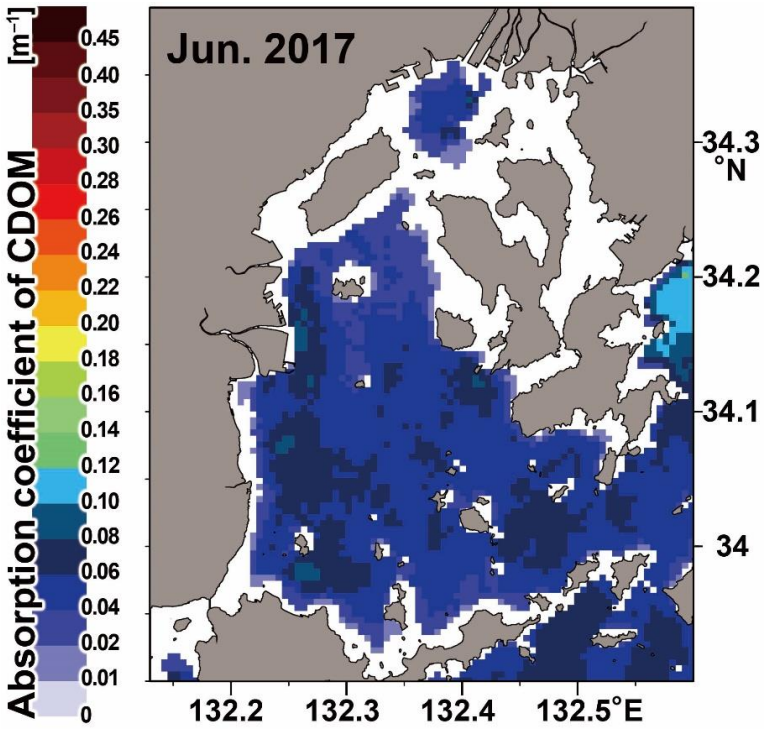


Fig. S14 CDOM in surface seawater in Jun 2017